Surv Geophys (2012) 33:169–209
DOI 10.1007/s10712-011-9118-2

Deep Electromagnetic Studies from Land, Sea, and Space: Progress Status in the Past 10 Years

A. V. Kuvshinov

Received: 29 November 2010 / Accepted: 2 March 2011 / Published online: 25 March 2011
© Springer Science+Business Media B.V. 2011

Abstract This review paper summarizes advances in deep electromagnetic studies of the Earth in the past decade. The paper reports progress in data interpretation, with special emphasis on three-dimensional and quasi one-dimensional developments, and results. The results obtained from data of different origin—geomagnetic observatories, long-period magnetotelluric experiments, submarines cables, and from low-Earth orbiting geomagnetic satellite missions—are described. Both frequency-domain and time-domain approaches are addressed. Perspectives for the future are also discussed.

Keywords Observatory, MT, cable, and satellite induction data · Electrical conductivity in the mantle · Water in upper mantle and transition zone · Sources of magnetospheric, ionospheric and oceanic origin · Global EM inversion · Multi-dimensional conductivity models · Frequency- and time-domain approaches

1 Introduction

Deep electromagnetic (EM) studies provide information on the mantle electrical conductivity at depths from the first hundreds kilometers down to (at best) the core-mantle boundary (2,900 km) and have been the focus of increasing interest during the last decade, mainly because of three reasons.

A primary reason is the recent growth in the amount of global geomagnetic data available, especially from low-Earth orbiting (LEO) satellite missions (Oersted, CHAMP and SAC-C). These satellites measure the magnetic fields from their circular orbits about the Earth with unprecedented accuracy. Moreover, the geomagnetic LEO three-satellite constellation mission *Swarm* is scheduled to be launched by the European Space Agency in 2012 (for details about these satellite missions the reader is referred to the review by Olsen et al. (2010)). In contrast to ground-based geomagnetic observatory data, which are sparsely and irregularly distributed with only a few located in oceanic regions,

A. V. Kuvshinov (✉)
Institute of Geophysics, ETH, 8092 Zurich, Switzerland
e-mail: kuvshinov@erdw.ethz.ch

satellite-borne measurements provide much better spatial coverage with high-precision data of uniform quality. In addition to satellite measurements, variations of voltage differences measured with the use of submarine cables also provide unique information in remote areas not otherwise accessible (cf. Lizarralde et al. 1995; Utada et al. 2003; Santos et al. 2003; among others).

A second reason is the great interest in the characterization of the three-dimensional (3-D) properties of the Earth's mantle on a global scale. One technique that has reached a level of maturity is seismic tomography, which can recover the 3-D variations in seismic wave speed in the mantle (cf. Becker and Boschi 2002; Romanowicz 2003; among others). This information is crucial in characterizing the dynamics of the mantle. For example, geodynamic processes such as mantle convection, the fate of subducting slabs and the origin of continents all have signatures in seismic wave speed. Although seismic tomography has proven important as a means of mapping mantle velocity heterogeneities, it suffers from the inability to separate effects arising from compositional and thermal variations (see e.g., Trampert et al. 2004; Khan et al. 2009). In this context deep EM studies—by recovering the electrical conductivity distribution in the mantle—provide independent and complementary information about the Earth's interior. This is indeed an important issue since conductivity reflects the connectivity of constituents as fluids, partial melt, and volatiles (all of which may have profound effects on rheology and, ultimately, mantle convection and tectonic activity), while seismology ascertains bulk mechanical properties. To deconvolve the relative effects of composition and temperature on mantle heterogeneities, or in illuminating the role of fluids (especially water) in the mantle, both methods are likely to be important.

The latter issue—to what extent the mantle is wet—is very topical because water content in the mantle not only governs physical rock properties but also transport properties such as viscosity, thermal and not least electrical conductivity (e. g. Karato 1990, 2006). However, debates are still continuing as to how effectively water enhances the electrical conductivity of mantle minerals. Experimental results with realistic mantle conditions have provided controversial results in terms of the effect of water on the major mantle minerals, such as olivine—the major mineral in upper mantle (to $\sim$410 km depth) (Yoshino et al. 2006; Wang et al. 2006), wadsleyite—the major mineral in upper part of transition zone (TZ; depth range 410–520 km), and ringwoodite—the major mineral in the lower part of the TZ (520–670 km depth) (Huang et al. 2005; Yoshino et al. 2008; Manthilake et al. 2009; Yoshino and Katsura 2009). While Yoshino and coauthors reported less effect from water in both upper mantle and TZ, Karato and coworkers claimed a larger effect (Karato and Dai 2009). Because the minerals in the TZ (i.e., wadsleyite and ringwoodite) are known to have a high H_20 solubility (up to $\sim$3 wt%, e.g., Inoue et al. 1995), the actual water content in the mantle transition zone is the key parameter to test the water filter hypothesis by Bercovici and Karato (2003).

Finally, recent interest in deep EM induction has also resulted from the significant methodological progress made during the last decade that has enabled accurate and detailed numerical calculations of induced magnetic and electric fields in 3-D spherical geometry. It is now possible to tackle various global induction problems involving high levels of complexity and spatial detail in both the electrical conductivity models and the sources. Recent progress in 3-D numerical modeling of EM signals at both ground and satellite altitude induced by a variety of realistic sources is reviewed by Kuvshinov (2008), while a new solver based on finite differences is presented by Weiss (2010).

The structure of the paper is as follows. Section 2 describes results based on ground-based data and data obtained with the use of submarine cables. This section is subdivided

in five subsections. Section 2.1 presents the reader with some essential details about the responses used in deep EM studies. Sections 2.2 and 2.3 summarize the results of regional 1-D and quasi 1-D deep EM studies. Sections 2.4 and 2.5 discuss the advances in 3-D inversion of long-period data in frequency and time domains. Section 3 outlines the results based on satellite data. This section has a similar structure as Sect. 2. Section 4 presents conclusions and Sect. 5 an outlook for future studies as seen by the author.

2 Deep EM Studies from Land and Sea

2.1 Response Functions Used in Deep EM Studies

In most EM studies, time series of hourly mean values of three geomagnetic field components have been used to recover electrical conductivity distributions in the mantle. These data are Fourier transformed, and then analyzed and interpreted in the frequency domain. The period range considered spans about four decades—from a few hours up to a few years. From the EM skin depth concept we know that this period range corresponds to the conductivities at depths between 200 and 2,000 km. Note that much attention has been paid in recent years to implementing a time-domain approach to global induction studies. This approach will be discussed later in the paper.

Depending on the period, two different sources are most frequently used for induction studies: (1) geomagnetic daily (periodic) variations with periods $24/p$ ($p = 1$–6) between 24 and 4 h, caused by electric currents flowing in the ionosphere at altitudes of ~ 110 km (Sq variations). The geometry of the source magnetic potential responsible for Sq variations is quite complex; moreover, the source geometry varies with period having a dominant term which is described by Y^p_{p+1} spherical harmonic function (see definition below); (2) geomagnetic (irregular) variations with periods longer than 1 day, caused by modulation of ring electric current in the magnetosphere (*Dst* variations). The geometry of the source magnetic potential responsible for *Dst* variations is simpler than for Sq variations and is dominated by Y^0_1 spherical harmonic function in the geomagnetic coordinate system. The longest periods of *Dst* variations are a few years. Several methods have been developed to infer the electrical conductivity of the Earth using Sq and *Dst* variations.

Analyzing these variations we rely on the solution of Maxwell's equations in frequency domain

$$\frac{1}{\mu_0}\nabla \times \mathbf{B} = \sigma \mathbf{E} + \mathbf{j}^{\text{ext}}, \tag{1}$$

$$\nabla \times \mathbf{E} = -i\omega \mathbf{B}, \tag{2}$$

where $\mathbf{E}$ and $\mathbf{B}$ are, respectively, time spectra of electric and magnetic fields, $\mathbf{j}^{\text{ext}}$ is (time spectrum of) the external current (source), σ is the conductivity distribution inside the Earth, $i = \sqrt{-1}$, the time factor is $e^{i\omega t}$, $\omega = 2\pi/T$, and T is period. Magnetic permeability is assumed to be that of free space, μ_0, everywhere. Displacement currents are ignored in the considered period range. Note that for time domain formulation the right hand side of Eq. 2 reads $-\frac{\partial \mathbf{B}}{\partial t}$. Another feature that distinguishes the frequency domain and time domain formulations is that the electric and magnetic fields are complex-valued and real-valued functions, respectively.

Above the conducting Earth ($r > a$, $a = 6{,}371.2$ km is Earth's mean radius) and beneath the external (for example, magnetospheric) sources, the Fourier component of the magnetic field, $\mathbf{B}(\omega) = -\text{grad}\, V(\omega)$, can be derived from a scalar magnetic potential, V, which obeys Laplace's equation, $\nabla^2 V = 0$, and which in spherical geometry can be represented by a spherical harmonic expansion

$$V = a \sum_{n,m} \left[\varepsilon_n^m(\omega) \left(\frac{r}{a}\right)^n + \imath_n^m(\omega) \left(\frac{a}{r}\right)^{n+1} \right] Y_n^m(\vartheta, \varphi), \tag{3}$$

where $\sum_{n,m}$ stands for the double sum $\sum_{n=1}^{\infty} \sum_{m=-n}^{n}$, r, ϑ and φ are, respectively, the distance from the Earth's center, co-latitude and longitude, ε_n^m and $\imath_n^m$ are the complex expansion coefficients of the external (inducing) and internal (induced) parts of the potential, $Y_n^m(\vartheta, \varphi) = P_n^m(\cos\vartheta) e^{im\varphi}$, and $P_n^m(\cos\vartheta)$ are associated Legendre polynomials of degree n and order m. Components of the magnetic field follow from the potential expansion and are given by

$$B_r = -\sum_{n,m} \left[n\varepsilon_n^m(\omega) \left(\frac{r}{a}\right)^{n-1} - (n+1)\imath_n^m(\omega) \left(\frac{a}{r}\right)^{n+2} \right] Y_n^m, \tag{4}$$

$$B_\vartheta = -\sum_{n,m} \left[\varepsilon_n^m(\omega) \left(\frac{r}{a}\right)^{n-1} + \imath_n^m(\omega) \left(\frac{a}{r}\right)^{n+2} \right] \frac{\partial Y_n^m}{\partial \vartheta}, \tag{5}$$

$$B_\varphi = -\sum_{n,m} \left[\varepsilon_n^m(\omega) \left(\frac{r}{a}\right)^{n-1} + \imath_n^m(\omega) \left(\frac{a}{r}\right)^{n+2} \right] \frac{1}{\sin\vartheta} \frac{\partial Y_n^m}{\partial \varphi}. \tag{6}$$

2.1.1 Potential Method

In this method the data collected *globally* are analyzed and Eqs. 4–6 are used to determine ε_n^m and $\imath_n^m$ by least squares. Then their ratio is estimated (cf. Schuster 1889; Chapman and Price 1930; among others). In the case of a radially-symmetric (1-D) conductivity distribution, i.e., $\sigma \equiv \sigma(r)$, each external coefficient induces only one internal coefficient (of the same degree n and order m) and their complex-valued ratio (Q-response) is independent of m

$$Q_n(\omega) = \frac{\imath_n^m(\omega)}{\varepsilon_n^m(\omega)}. \tag{7}$$

In this case Eq. 3 can be rewritten as

$$V = a \sum_{n,m} \left[\varepsilon_n^m(\omega) \left\{ \left(\frac{r}{a}\right)^n + Q_n(\omega) \left(\frac{a}{r}\right)^{n+1} \right\} \right] Y_n^m. \tag{8}$$

If $Q_n(\omega)$ is known for a set of frequencies, a globally averaged 1-D conductivity can be constructed. Recent applications of the method are discussed by Schmucker (1999a, b) who analyzed Sq signals, and by Constable and Constable (2004), and Kuvshinov and Olsen (2006), who dealt with *Dst* signals. The generalization of the Q-response concept to a 3-D case is presented in Sect. 3.3.

It is relevant to mention that from Eqs. 4–6 it follows that the radial component is to a greater extent relative to the horizontal components influenced by induction. Indeed, for

the horizontal components the degree of this influence is governed by the Q-response itself. For the radial component, the degree of the influence is governed by the quantity

$$Q_n^{(r)}(\omega) \equiv \frac{n+1}{n} Q_n(\omega), \tag{9}$$

which implies that the relative amount of induction (compared with the external part) in the radial component is $(n + 1)/n$ times larger for individual terms than for the horizontal components. In addition, due to subtraction in the radial component, the ratio of induced signal to total (external + induced) signal is much larger (because the total signal tends to 0 for the radial field).

Figure 1 presents $|Q_n^{(r)}|$ for a range of periods as a function of harmonic of degree n for some typical global 1-D conductivity profile (with and without ocean). Solid black lines below the plot show the range of degree n of the different sources. For comparison, the dotted line in the plot shows an upper limit of 1, for $|Q_n^{(r)}|$, which corresponds to a perfectly conducting Earth. In this case, induction cancels the radial component at the surface of the Earth and more or less doubles the horizontal component. For all n, we observe that the longer the period the smaller $|Q_n^{(r)}|$. In addition, $|Q_n^{(r)}|$ also decreases with increasing of n. For example, at a period of 24 h $|Q_n^{(r)}|$ drops from 0.56 for $n = 2$ (degree of fundamental spherical harmonic of Sq at this period) down to less than 0.03 for $n = 20$, when inland (without ocean) 1-D profile is considered. The latter result is very important since it means that one cannot expect an induction signal from the polar electrojet (requiring $n \geq 20$) at periods longer than a few days. Contamination of deep EM results by the polar electrojet will be discussed later in the review.

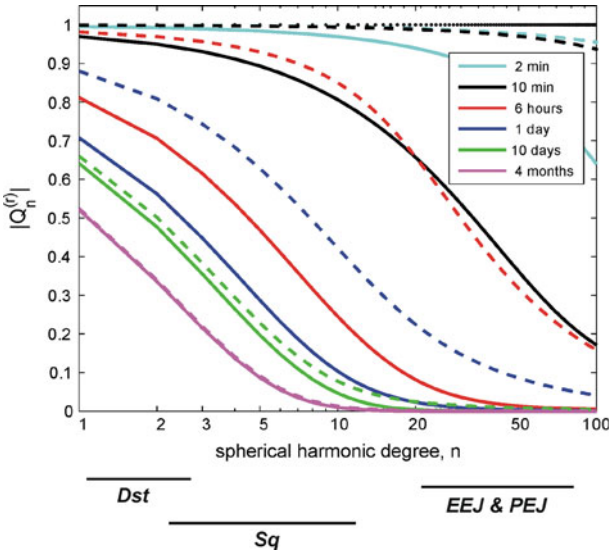

Fig. 1 $|Q_n^{(r)}|$ for different periods as a function of degree n. *Solid lines* $|Q_n^{(r)}|$ for a typical global 1-D conductivity profile. *Dashed lines* $|Q_n^{(r)}|$ for the same 1-D model overlain by a uniform ocean of 15,000 S. For comparison, the *dotted line* in the figure shows an upper limit, 1, for $|Q_n^{(r)}|$ which corresponds to a perfectly conducting Earth. After Kuvshinov (2008)

2.1.2 GDS Method

If the source magnetic potential can be described by a single spherical harmonic function, $Y_1^0 \equiv P_1^0 = \cos\vartheta_d$, and if the Earth is assumed to be regionally 1-D, then the C-response can be introduced at a given site (Banks 1969)

$$C(\omega) = -\frac{a \tan\vartheta_d B_r(\omega)}{2 \quad B_\vartheta(\omega)}, \tag{10}$$

where ϑ_d is the geomagnetic co-latitude. The complex-valued C-response has physical dimension of length and for 1-D conductivity models its real part provides an estimation of the depth to which EM field penetrates (Weidelt 1972). This technique of estimating C-responses will be referred below as the geomagnetic depth sounding (GDS) method. There is a common consensus that it works fairly well in period range between a few days and a few months (cf. Banks 1969; Roberts 1984; Schultz and Larsen 1987; Fujii and Schultz 2002; among others), thus allowing for the recovery of electrical conductivities in depth range from 400 to 500 km down to 1,500 km.

Note that the C-response is closely related to the 1-D magnetotelluric impedance

$$Z(\omega) = i\omega C(\omega). \tag{11}$$

Also note that often researchers work with apparent resistivity and impedance phase

$$\rho_a = \omega\mu_0|C|^2, \tag{12}$$

$$\phi = \arg\{Z\} = \frac{\pi}{2} + \arg\{C\}, \tag{13}$$

rather than with C-responses themselves.

If the Earth is assumed to be 1-D globally then C-response at the Earth's surface is related to Q_1 as

$$C(r = a, \omega) = -\frac{a}{2}\frac{1 - 2Q_1(\omega)}{1 + Q_1(\omega)}. \tag{14}$$

2.1.3 HSG Method

If the source is described by more than one spherical harmonic (this is generally true for the variations with periods smaller than a few days, for example, for Sq variations) then the so-called horizontal spatial gradient (HSG) method is usually applied (Schmucker 1970, 1979; Olsen 1998; among others) to determine C-responses. Using this method the C-response is calculated as

$$C = -\frac{B_r}{\nabla_\tau \cdot \mathbf{B}_\tau}, \tag{15}$$

where $\nabla_\tau \cdot \mathbf{B}_\tau$ is the angular part of divergence (horizontal divergence). In reality, one doesn't directly measure spatial derivatives of the field. The common practice while applying the HSG method is to interpolate the field using low-order polynomials or spherical harmonics and then analytically estimate the derivatives. Since the global net of geomagnetic observatories is strongly irregular such an approach to approximating $\nabla_\tau \cdot \mathbf{B}_\tau$ works reasonably well only for Europe where the spatial coverage is rather dense and uniform. Finally, due to the "low-order" approximation used to determine $\nabla_\tau \cdot \mathbf{B}_\tau$, $\nabla_\tau \cdot \mathbf{B}_{\tau,n}$

is actually determined, where $\mathbf{B}_{\tau,n}$ is the smoothed (normal) part of the horizontal components.

2.1.4 HSG + GDS Method

The main limitation of the approaches described in Sects. 2.1.2 and 2.1.3 is that they have been designed to deal with 1-D conductivity models of the Earth. Recently Schmucker (2003) presented a generalization of this approach that removes the constraint about one-dimensionality. In a case of moderate 3-D induction anomalies a new relation is introduced, which locally connects the radial magnetic component with the angular part of the divergence of the normal horizontal components and the normal horizontal components themselves

$$B_r \approx -C\nabla_\tau \cdot \mathbf{B}_{\tau,n} + z_H \mathbf{B}_{\vartheta,n} - z_D \mathbf{B}_{\varphi,n}. \tag{16}$$

It is seen from Eq. 16 that in order to determine transfer functions C, z_H, z_D—in addition to the constraint of good regional coverage to compute $\nabla_\tau \cdot \mathbf{B}_{\tau,n}$—source fields of sufficient spatial and temporal variability are required to guarantee robust determination of three responses. Moreover the linear independence between the horizontal divergence and two orthogonal horizontal components should be satisfied (i.e., they should be incoherent to each other) for the robust estimates of the responses. This, in particular, means that the application of the method is limited to periods smaller than a few days, because at longer periods the single term, Y_1^0, is dominating. A similar approach is also discussed in papers of Vozar and Semenov (2010) and Semenov and Shuman (2010). However these authors use the total field instead of the normal field in the right hand side of Eq. 16.

2.1.5 Long-Period Magnetotelluric (MT) Responses

If, along with magnetic field measurements, the horizontal electric field is measured, conventional MT responses, $Z_{ij}(i,j = \vartheta,\varphi)$ can be estimated using

$$E_\vartheta = Z_{\vartheta\vartheta}B_\vartheta + Z_{\vartheta\varphi}B_\varphi, \tag{17}$$

$$E_\varphi = Z_{\varphi\vartheta}B_\vartheta + Z_{\varphi\varphi}B_\varphi. \tag{18}$$

The use of electric fields gives an opportunity the responses at periods shorter than a few days can be obtained which provides information on conductivities at depths shallower than 400–500 km. Another merit of the MT technique is that it works in regions where the GDS method fails. For example, MT measurements might be helpful in the vicinity of the geomagnetic equator where B_r of magnetospheric origin is close to zero thus preventing the usage of the GDS method. High latitudes are also favorable for MT experiments since in these regions GDS responses suffer from strong contamination by non-P_1^0sources.

However, since the strength of electric field signals drop dramatically as the period increases, and due to the long-term drift of the electrodes, that are used to measure electric field, it is rather difficult to obtain good quality MT responses at very long periods. As far as is known the period of 10 days is the longest period at which reliable MT responses have been obtained so far (cf. Utada et al. 2003). Another problem with the MT method is the so-called static shift of the responses (cf. Jiracek 1990) which is generally non-trivial to correct for.

2.1.6 Other Responses

D- and *K*-ratios were introduced by Fujii and Schultz (2002) and Shimizu et al. (2009), respectively, to deal with global 3-D Earth's models. Although these ratios are potentially useful, they are not, strictly speaking, response functions in the common sense due to their inherent dependence on the source, and will not be discussed further.

2.2 Regional 1-D Studies

During the last decade a number of studies have estimated mantle 1-D conductivity profiles in different regions of the world by inverting the responses described above. Most of the studies employed the regularized Occam's method of Constable et al. (1987) to invert the responses.

Olsen (1998), using data from 24 European observatories, obtained European averaged *C*-responses in the period range between 3 h and 1 month. The so-called *Z:Y* approach (a modification of the HSG method) was used to estimate *C*-responses, which means that the vertical component is taken locally whereas horizontal components are used globally by expansion in a series of spherical harmonics. The author noted that a good description of the source structure is essential for the determination of good responses. Later Olsen (1999a) extended the methodology to obtain averaged *C*-responses for periods between 1 month and 1 year. In both studies a special effort was made to obtain unbiased estimates of the responses. His responses have been employed in several studies seeking to infer information about the Earth's mantle structure.

Neal et al. (2000) analyzed long-period MT and GDS data from diverse tectonic regions in North America and the Pacific Ocean. Specifically, they obtained 1-D conductivity profiles beneath Carty Lake (CLC) in the Canadian Shield, Tucson (TUC) in the South West United States, Honolulu (HON) and Midway (MID) in the North central Pacific. They found significant lateral variations in conductivity associated with the various tectonic settings. In particular, upper mantle beneath Carty Lake appeared to be approximately an order of magnitude more resistive than the upper mantle beneath Tucson and nearly 1.5 orders of magnitude more resistive than Honolulu and Midway Island. The authors speculated that the observed conductivity variations may be interpreted as lateral variations in temperature, partial melt and/or dissolved hydrogen in olivine.

Ichiki et al. (2001) reported a 1-D conductivity model of the upper mantle including TZ beneath the Pacific back-arc of North East China. The conductivity structures were investigated through long-period MT and GDS experiments. The electric field data were acquired using land telephone lines to obtain MT responses at three different (but close) locations. GDS responses were obtained using Changchun (CHN) geomagnetic observatory data. The authors compared their profiles with those at CLC, TUC and HON. The most distinct difference revealed in their study was that the TZ beneath North East China is significantly more conductive than the others by about one order of magnitude. This led the authors to suggest that the high conductivity is most probably related to the presence of water in the stagnant slab. For depths shallower than 400 km, their conductivity profile has a slope and conductivity values similar to TUC, which is also more conductive than observed elsewhere. Ichiki et al. (2001) noted that this common feature is probably typical of the continental upper mantle beneath the region of active tectonics as also pointed out by Neal et al. (2000).

Tarits et al. (2004) presented the results of long-period MT sounding in the French Alps from which a vertical electrical conductivity profile between 200 and 1,000 km was

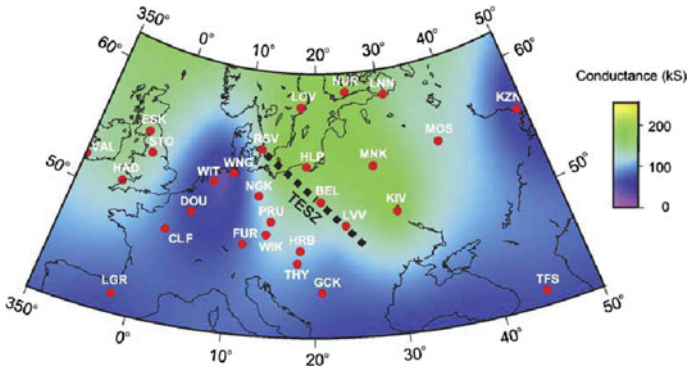

Fig. 2 Smoothed image of the integrated conductance, in kilosiemens, from the surface down to the depth of 770 km in the mantle beneath Europe. After Semenov and Jozwiak (2006)

obtained. They concluded that for depths between 200 and 400 km their model favors a wet mantle. The authors noticed that the data do not require the conductivity to change throughout the TZ; conductivity in TZ is at least one order of magnitude smaller compared with the conductivity reported by Ichiki et al. (2001) suggesting that little water has been transported into the TZ by the subduction in the Mediterranean.

Semenov and Jozwiak (2006) compiled the response functions for 35 European observatories in the period range between 6 h and 11 years using various data sets including data by Roberts (1984), Schultz and Larsen (1987) and Olsen (1998). The combined responses have been inverted individually and the resulting 1-D profiles have been merged to obtain a mantle conductance image down to a depth of $\sim$800 km (see Fig. 2). The authors noticed that their conductance image can be correlated with major European tectonic units like the Baltic Shield and the Trans-European Suture zone (TESZ).

Khan et al. (2006) re-inverted Olsen's data set to constrain the thermo-chemical state of Earth's mantle. In contrast to the standard approach when responses are inverted for conductivity profiles, authors went beyond this methodology by inverting the responses directly for chemical composition and thermal state of the Earth. Given these parameters they calculated mineral modes at the prevailing physical conditions and combine these with laboratory-based models for the conductivity of individual minerals to estimate the bulk Earth electrical conductivity structure from which *C*-responses are calculated. Also in contrast to conventional (deterministic) inversion schemes the authors exploited a probabilistic approach using a stochastic-based sampling algorithm (e.g., Mosegaard 1998). The advantage of the probabilistic approach lies in its inherent ability to fully incorporate nonlinearities into the final solution, obviating any form of linearization of the original problem that is typical of deterministic approaches. Their results agreed with earlier derived conductivity and seismic velocity models and confirmed that direct inversion of EM data is feasible.

Medin et al. (2007) re-inverted Olsen data using a non-traditional inverse approach, the so called "all-at-once" method (e.g., Haber et al. 2004). In this method the forward modeling equations are constraints in an optimization problem solving for the electric fields and the conductivity simultaneously. There is no regularization required to solve the problem. The method provides bounds on Earth's average conductivity that all conductivity profiles must satisfy. By further comparing inversion results with laboratory results, the authors were able to place constraints on temperature and water content in the upper

mantle and TZ. Regarding water content authors concluded that with their bounds on conductivity, a transition zone consisting entirely of wadsleyite has <0.27 wt% water and by adding in a fraction of ringwoodite, the upper bound on water content decreases proportionally. This water content is less than the 0.4 wt% water required for melt or pooling at the 410 km seismic discontinuity.

Toffelmier and Tyburczy (2007) re-interpreted MT and GDS data of Egbert et al. (1992) at Tucson (TUC) by incorporating the effect of melt in TZ. In contrast to previous studies they did not invert the data but constructed mineral-physics-based electrical conductivity profiles of the upper mantle and TZ consistent with seismic constraints for the region of interest. Authors noticed that the agreement between forward models and Tucson MT/GDS data is enhanced when a thin melt (of 5–30 km thickness) layer of conductance 3×10^4 S at 410 km is added to the regional 1-D conductivity profile. However, their results are not entirely convincing as their preferred conductivity model did not fit the part of the responses (within uncertainties) which is mainly sensitive to upper mantle and TZ structure.

Khan et al. (2010) investigated the electrical conductivity structure of the mantle at six different locations around the globe that cover different geological settings. The selected observatories were: Fuerstenfeldbrueck (FUR), Europe; Hermanus (HER), South Africa; Langzhou (LZH), China; Alice Springs (ASP), Australia, Tucson (TUC), North America and Honolulu (HON), North Pacific. They inverted the response functions beneath each observatory for a local 1-D conductivity profile using a probabilistic approach already successfully implemented in earlier work of Khan et al. (2006). Resolution is limited to the 500–1,200 km depth. The authors found large variations in conductivity throughout the depth range studied. Mean conductivity varies between 0.1 and 0.4 S/m at 600 km depth, with a marked increase in conductivity (1.3–2.0 S/m) occurring at 800 km depth for all stations except HER (0.5 S/m). Conductivity at 900 km depth increases further to 1.4–2.4 S/m with HER, HON and ASP being most conductive. This trend persists to a depth of 1,200 km. A comparison with conductivity profiles constructed from the most recent laboratory mineral conductivity measurements and models of Earth's mantle composition and thermal state revealed that significant variations in mantle composition and temperature are at the origin of the observed heterogeneous mantle conductivity structure. The authors remarked that due to the somewhat large error bounds on sampled conductivity profiles and the reduced sensitivity of their responses in the upper mantle and TZ, constraints on transition zone water content are not conclusive.

2.3 Semi-Global Quasi 1-D Studies

In all studies discussed in the previous section (except for the study of Khan et al. (2010)), various but 1-D interpretation schemes were used to obtain local/regional profiles. The study of Utada et al. (2003) commenced *quasi* 1-D studies (continued by Kuvshinov et al. 2005 and Shimizu et al. 2010a), which aimed at obtaining semi-global 1-D mantle electric conductivity structure beneath the North Pacific using 3-D modeling of the ocean effect. It is well recognized that the ocean has a large influence on the coastal responses (cf. Kuvshinov et al. 1999, 2002). Kuvshinov et al. (2002) demonstrated that a nonuniform ocean is a major contributor to the anomalous behavior of the C-responses at coastal observatories up to periods of 20 days. Kuvshinov et al. (2002) also showed that the effects arising from the oceans may be corrected for by multiplying the observed response, C, by the ratio of the synthetic response 1-D Earth's model (without oceans), C^{1D}, with the

response of the same 1-D Earth overlain by an inhomogeneous ocean of known conductance, $C^{1D+ocean}$

$$C^{exp,\,corr} = C^{exp} \cdot \frac{C^{1D}}{C^{1D+ocean}}. \tag{19}$$

Here C^{exp} and $C^{exp,corr}$ are observed and corrected C-responses, respectively. Utada et al. (2003) suggested an iterative correction based on a similar procedure, and showed that with a few iterations good agreement between observed and predicted responses can be achieved.

Utada et al. (2003) (and later Kuvshinov et al. 2005 and Shimizu et al. 2010a) used this technique to obtain reference 1-D structures beneath the North Pacific. Further discussion in this section is based on the most recent results of Shimizu et al. (2010a). Their procedure to obtain a reference 1-D profile consists of four steps: (a) estimation of the responses obtained from 13 geomagnetic observatories and 8 transoceanic submarine cables (see their location in Fig. 3); (b) correction of the responses using Eq. 19 with a given 1-D conductivity model; (c) averaging of the corrected responses to obtain composite quasi-1-D response; (d) 1-D inversion of the composite response; (e) an iteration of the procedure from step (b) with the new 1-D conductivity profile until convergence is achieved.

Assuming P_1^0 excitation, scalar cable MT responses are calculated in their study as

$$Z_{cab}(\omega) = -\frac{\mu_0 V(\omega)}{L B_\vartheta^{ref}(\omega) \sin\alpha} \frac{\sin\vartheta_{ref}}{\sin\vartheta_{cab}}. \tag{20}$$

Here V is the voltage measured by a submarine cable between its end points, L is the length of the cable, B_ϑ^{ref} is the directed toward geomagnetic South component at a reference observatory (specifically, Kakioka in their study), α is the azimuth angle of the cable with respect to geomagnetic North, ϑ^{ref} and ϑ^{cab} are the geomagnetic colatitudes of the reference observatory and the mid-point of the cable, respectively. The experimental responses in the period range from 1.7 to 113 days were used to construct the reference 1-D model. The authors examined three different models of conductivity variation with depth: (1) a model with no discontinuities; (2) a model with two jumps at 400 and 650 km depths; and (3) a model with three jumps at 400, 500 and 650 km depths. Figure 4 compares their two-jump model with the two-jump models by Utada et al. (2003) and Kuvshinov et al. (2005).

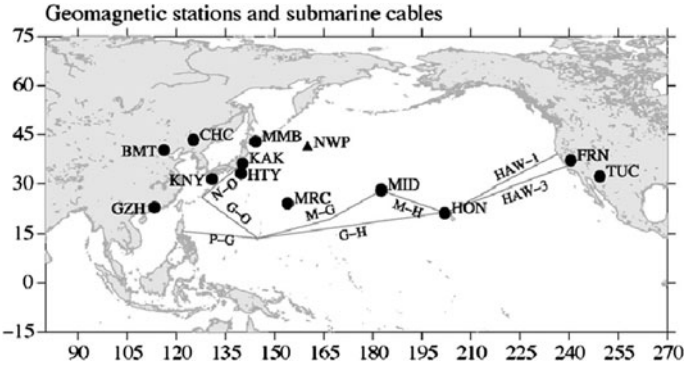

Fig. 3 Distribution of the magnetic stations and submarine cables from which data were collected and used to obtain the electrical conductivity structure beneath North Pacific. After Shimizu et al. (2010a)

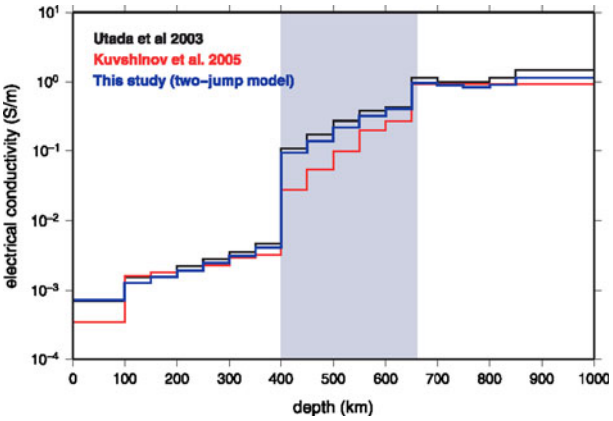

Fig. 4 Comparison of the two-jump model beneath the North Pacific obtained by Utada et al. (2003) (*black line*), by Kuvshinov et al. (2005) (*red line*) and by Shimizu et al. (2010b). After Shimizu et al. (2010a)

The authors concluded that the conductivity of the two-jump model in the transition zone is higher than the experimentally determined conductivity of dry wadsleyite and ringwoodite. If the difference is entirely due to the effect of water in the transition zone, then the conductivity is consistent with water content around 0.5 wt%. However, if an additional discontinuity of electrical conductivity is allowed at the 500 km depth, the obtained conductivity for the upper 100 km of the transition zone is lower, and can be explained by a water content of 0.1 wt% in wadsleyite.

2.4 Global (and Semi-Global) 3-D Inversions in Frequency Domain

The first attempt to invert global induction data in a 3-D frame was performed by Schultz and Pritchard (1999). Their study was based on inversion of the augmented Schultz and Larsen (1987) set of *C*-responses. Their *approximate* forward modeling approach used for this inversion was accurate only for small perturbations about a reference 1-D model, and it was found that no model satisfying this limitation could fit the European subset of observatories.

Later on, three *rigorous* frequency-domain 3-D global EM inverse solutions to deal with ground-based data have been developed independently at the Earthquake Research Institute (Tokyo University, Japan), Oregon State University (Corvallis, USA), and Institute of Geophysics (ETH, Zurich, Switzerland). Their solutions were explained and applied to real data in a number of publications/presentations (cf. Koyama 2001; Fukao et al. 2004, Koyama et al. 2006; Kelbert et al. 2008, 2009a, b; Kuvshinov et al. 2008; Utada et al. 2009; Shimizu et al. 2010b; Semenov and Kuvshinov 2010) which are summarized below.

Although differing in detail all existing frequency-domain 3-D EM global inversions possess the following common features.

First, in all approaches the regularized least-squares inverse problem is solved. Thus the inverse problem is formulated as an optimization problem, so that

$$\phi(\mathbf{m}, \lambda) \underset{\mathbf{m}}{\rightarrow} \min, \tag{21}$$

where a penalty functional, $\phi(\mathbf{m}, \lambda)$ is defined as a sum of misfit, ϕ_d $(\mathbf{m})$, and regularization, ϕ_R $(\mathbf{m})$, terms

$$\phi(\mathbf{m}, \lambda) = \phi_d(\mathbf{m}) + \lambda \phi_R(\mathbf{m}). \tag{22}$$

where

$$\phi_d = \sum_{\omega \in \Omega} \sum_{\mathbf{r}_a \in \text{Sites}} D(\omega, \mathbf{r}_a) |\Phi(\mathbf{m}, \omega, \mathbf{r}_a) - \Phi^{\text{exp}}(\omega, \mathbf{r}_a)|^2, \tag{23}$$

and

$$\phi_R(\mathbf{m}) = (W(\mathbf{m} - \mathbf{m}_0))^T W(\mathbf{m} - \mathbf{m}_0). \tag{24}$$

Here $\mathbf{m}$, $\mathbf{m}_0$ are vectors representing, respectively, the model parameters (describing 3-D conductivity distribution in the model) and the a priori (as usual 1-D) model, $\Phi(\mathbf{m}, \omega, \mathbf{r}_a)$ and $\Phi^{\text{exp}}(\omega, \mathbf{r}_a)$ are predicted and observed responses, respectively, $D(\omega, \mathbf{r}_a)$ is the inverse of the squared uncertainties of the observed responses. Note that $\Phi(\mathbf{m}, \omega, \mathbf{r}_a)$ depends non-linearly on $\mathbf{m}$ and $\mathbf{m}_0$. In addition W is the regularization matrix which—together with the damping parameter λ—controls model smoothness; the subscript T denotes the transpose. The sum is over all sites (observatories) and frequencies.

Second, numerical solutions of Maxwell's equations (1)–(2) (forward modeling) that are needed to calculate the predicted responses (and gradients of the misfit with respect to model parameters) during the inversion are obtained in a *spherical* geometry.

Third, due to the large number of parameters in the 3-D EM inverse problems, iterative *gradient-type* optimization methods (cf. Nocedal and Wright 2006), such as quasi-Newton (QN) method or non-linear conjugate gradients (NLCG), are employed to minimize a penalty functional.

Fourth, in order to efficiently calculate the misfit gradients with respect to model parameters an *adjoint* approach (cf. Mackie and Madden 1993; Rodi and Mackie 2000; Kelbert et al. 2008; among others) is invoked. The adjoint approach allows for the calculation of the misfit gradient for the price of only a few additional forward predictions per period with a specific (adjoint) source. Note that each inverse problem setting requires the finding of explicit formulas for the adjoint source. Pankratov and Kuvshinov (2010) presented a general formalism for the efficient calculation of the derivatives of EM frequency-domain responses and the derivatives of the misfit with respect to variations of 3-D isotropic/anisotropic conductivity. Using this formalism one can readily obtain appropriate formulae for the specific sounding methods. To illustrate the concept the authors provided these formulae for a number of EM techniques including GDS, HSG and HSG + GDS.

Fifth, most of the studies exploit *checkerboard* tests for resolution analysis. As was shown by Shimizu et al. (2009) this test was indeed able to reveal the resolution of the individual heterogeneous blocks which compose the checkerboard pattern.

Sixth, in all 3-D inversions performed so far only the signals originating from *magnetospheric* ring current are considered. Moreover *dipolar* characteristics of this current are assumed, i.e., the source magnetic potential is described by a single spherical harmonic function in the *geomagnetic* coordinate system. As already mentioned this assumption is valid for signals with periods longer than a few days and allows the use of local *C*-responses obtained by the GDS method.

Seventh, in most inversions a nonuniform surface layer of known conductance was included in the model to account for the ocean effect (or corrected for it as it was done by Kelbert et al. (2009a, b)).

Koyama (2001) pioneered the development and application of a rigorous 3-D inversion scheme to interpret ground-based *C*-responses on a (semi) global scale. His inversion

exploits a quasi-Newton optimization method whereas the forward solver is based on a modern version of the volume integral equation (IE) approach (cf. Singer 1995; Pankratov et al. 1995, see also, Kuvshinov 2008). In his implementation vector $\mathbf{m} - \mathbf{m}_0$ has the form

$$\mathbf{m} - \mathbf{m}_0 = \left[\ln(\sigma_1/\sigma_1^0),\, \ln(\sigma_2/\sigma_2^0), \ldots,\, \ln(\sigma_N/\sigma_N^0)\right]^T, \tag{25}$$

where σ_i $(i = 1, 2, \ldots, N)$ are the unknown conductivities in ith block (cell) of the inversion domain, and σ_i^0 are the conductivities of an a priori 1-D model.

In subsequent studies (Fukao et al. 2004; Koyama et al. 2006; Utada et al. 2009; Shimizu et al. 2010b) his 3-D inverse solution was used to interpret long-period EM data, mostly in the North Pacific region (termed semi-global studies). In all these investigations voltage data from trans-Pacific submarine cables and magnetic field data from circum-Pacific geomagnetic observatories were analyzed (see again Fig. 3). The exception is the study of Utada et al. (2009) where data from Europe were analyzed (to be discussed later in this section). In addition, in the above studies lateral heterogeneity was assumed to exist between 350 and 850 km depth, with the aim of resolving the electrical conductivity structures in and around the TZ.

Fukao et al. (2004) performed independent EM and seismic inversions in the North Pacific region and compared anomaly maps of *P*-wave velocity with those of electrical conductivity at four different depths in the TZ (see Fig. 5). The GDS responses at 8 periods from 5.3 to 28.4 days and MT cable responses at 8 periods from 1.3 to 7.2 were chosen for the 3-D inversion. The 1-D conductivity model beneath the North Pacific obtained by Utada et al. (2003) was employed as the reference and starting models for inversion. The grid spacing for the calculating forward problem was $2^\circ \times 2^\circ$ laterally and 50 km radially. The size of each block in the inversion domain was $15^\circ \times 15^\circ$ laterally and 100 km radially, amounting to a total of $N = 12 \times 6 \times 5$ unknowns. The normalized misfit was reduced by 30% after running the inversion for 11 iterations.

Conductivity maps revealed two features: (1) a high conductivity anomaly beneath the Philippine Sea and above the penetrated slab, and (2) a high conductivity anomaly beneath Hawaii. The authors discovered a correlation between high- (low-) velocity anomalies and low- (high-) conductivity anomalies, although they noted that correlation is not always perfect. Fukao et al. (2004) claimed that, where such a correlation exists, one may invoke a thermal origin for the observed velocity and conductivity anomalies. Assuming tentatively that all the anomalies are of thermal origin they converted the recovered heterogeneous conductivity and velocity structures to temperature anomalies using

$$\delta T_{3\mathrm{D}} = -k\frac{\delta V_{3\mathrm{D}}}{V_{1\mathrm{D}}}, \tag{26}$$

where k is a depth-dependent conversion factor proposed by Karato (1993) and based on mineral physics data, $\delta T_{3\mathrm{D}}$ and $\delta V_{3\mathrm{D}}$ are lateral temperature and velocity deviations from the 1-D temperature and velocity distributions, $T_{1\mathrm{D}}$ and $V_{1\mathrm{D}}$, respectively. For $V_{1\mathrm{D}}$ a standard 1-D P-wave velocity model was used (Kennett and Engdahl 1991) and for $T_{1\mathrm{D}}$ the simplest and the smoothest model of Ito and Katsura (1989)

$$T_{1\mathrm{D}} = 0.5d + 1500, \tag{27}$$

was adopted, where T and d are measured in K and km, respectively. Conductivity-to-temperature conversion was performed as follows

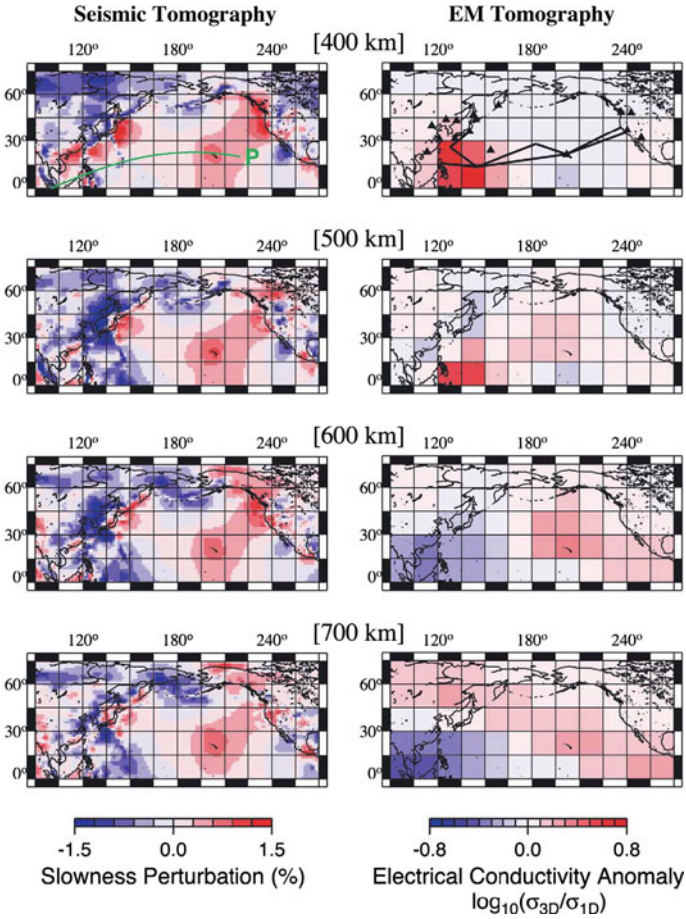

Fig. 5 *Left P*-wave velocity perturbations (Fukao et al. 2003). High- and low-velocity anomalies are colored *blue* and *red*, respectively, in linear scale. Tomographic cross-sections were taken along profile *P*. *Right* electrical conductivity perturbations. High- and low-conductivity anomalies are colored *red* and *blue*, respectively, in logarithmic scale. After Fukao et al. (2004)

$$\frac{\delta T_{3D}}{T_{1D}} = -\frac{\ln(\sigma_{3D}/\sigma_{1D})}{\ln(\sigma_{1D}/\sigma_0)}, \tag{28}$$

where σ_{1D} is the 1-D conductivity model obtained by Utada et al. (2003) and used as starting model to construct the 3-D conductivity model, σ_{3D}; σ_0 is the pre-exponential term of an Arrhenius formula for the representative mantle material in the relevant depth range (see Eq. 29 below). For σ_0 the authors used the geometric mean of the laboratory values for wadsleyite and ringwoodite (Xu et al. 1998).

Figure 6 shows cross-sections for the temperature perturbations δT_{3D} calculated by formulas (26) and (28) respectively. Fukao et al. (2004) found that their cross-sections beneath Hawaii between 400 and 800 km depth was anomalously hot (with anomalies of order 200–300 K at a lateral scale of 1,000 km), a feature which is consistent with the results from both seismic and EM inversions. The lack of quantitative agreement between

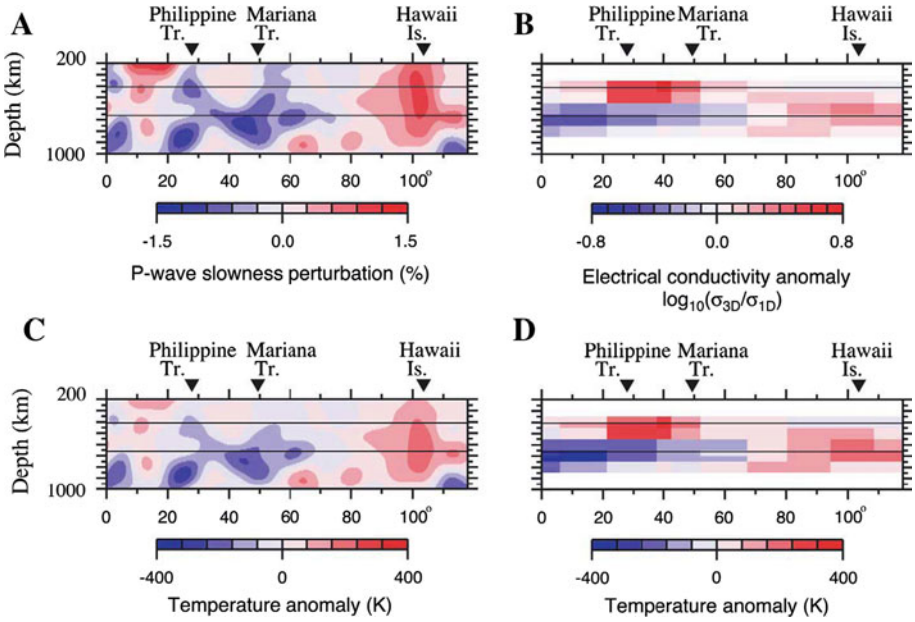

Fig. 6 Cross-sections along profile P across Hawaii and Philippine Sea. See upper left plot of Fig. 5 for the location of the profile P. **a** *P*-wave velocity anomalies at depths 200–1,000 km. **b** Electrical conductivity anomalies at depths 350–850 km. **c** Temperature anomalies converted from *P*-wave velocity anomalies. **d** Temperature anomalies converted from electrical conductivity anomalies. After Fukao et al. (2004)

the EM and seismic results in Philippine Sea region was suggested to require a cause other than temperature.

This was further investigated by Koyama et al. (2006), who suggested that the high conductivity anomaly beneath Philippine Sea is due to the effect of water (or hydrogen) in wadsleyite. They estimated the amount of water in the mantle transition zone in the western Pacific to be 0.3 wt% using the diffusivity of hydrogen obtained experimentally by Hae et al. (2006).

Utada et al. (2009) detected regional differences between North Pacific 3-D conductivity model and 3-D conductivity model beneath Europe. They inverted GDS *C*-responses obtained in the period range between 5 and 50 days from 12 selected European observatories (see location of the observatories in Fig. 7). Again, the 1-D model for the North Pacific region (Utada et al. 2003) was used as the reference model. The grid spacing for the forward problem calculations was $1^\circ \times 1^\circ$ laterally and 50 km radially. The size of each block in the inversion domain was $5^\circ \times 5^\circ$ laterally and 100 km radially, resulting in a total of $N = 9 \times 9 \times 5$ unknowns. No regularization was applied during inversion. The inversion required 40 iterations and reduced the normalized misfit from 5.50 to 1.39.

Figure 8 shows the derived conductivity anomaly maps as well as the results of global *P*- and *S*-wave tomography (Obayashi et al. 2006; Megnin and Romanowicz 2000). The authors find that the most notable feature in their results (see Fig. 8) is the correlation between the low-conductivity and high-velocity anomalies beneath the central part of Europe, where slab material subducted from the Tyrrhenian trench stagnates in the TZ (Faccena et al. 2003). They claim that such correlation implies that the low-conductivity and high-velocity characteristics of the stagnant slab (Fukao et al. 2001) have a common

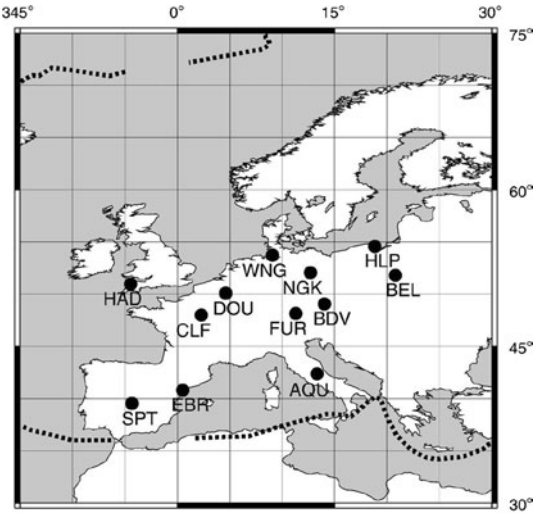

Fig. 7 Locations of 12 selected geomagnetic observatories in Europe. Major plate boundaries are indicated by *dotted lines*. After Utada et al. (2009)

origin, most likely temperature, and thus that there is no need to assume an additional conduction mechanism (e.g., hydrogen conduction) as implemented for the western Pacific region (Koyama et al. 2006) to explain a particular conductivity anomaly. These results led the authors to infer that TZ beneath Europe is relatively dry.

To verify this they performed quantitative analyses of the independent data sets. First they converted velocity anomalies $\delta V_P(r,\vartheta,\varphi)$ and $\delta V_S(r,\vartheta,\varphi)$ in each block of their inversion domain into temperature anomalies $\delta T_P(r,\vartheta,\varphi)$ and $\delta T_S(r,\vartheta,\varphi)$ using Eq. 26. The logarithm of 3-D conductivity, $\ln\sigma_{3D}(r,\vartheta,\varphi)$, for each block was then plotted against $1/(T_{1D}+\delta T_P(r,\vartheta,\varphi))$ and $1/(T_{1D}+\delta T_S(r,\vartheta,\varphi))$ (see Fig. 9). The reasoning to plot the quantities in such a way follows from Arrhenius relation

$$\sigma = \sigma_0 \exp\left(-\frac{H}{kT}\right), \tag{29}$$

which a logarithmic scale implies a linear relation between $\ln\sigma$, and inverse of temperature, $1/T$

$$\ln\sigma = a - b\frac{1}{T}, \tag{30}$$

Here $a = \ln\sigma_0$, $b = H/k$, σ_0 is a pre-exponential term, H is activation enthalpy and k is Boltzmann's constant.

Figure 9 presents conductivity-temperature relations beneath Europe, and for comparison, beneath the Philippine Sea. Predictions from experimental data for both dry and water-containing wadsleyite and ringwoodite (Yoshino et al. 2008) are also shown in the figure. Utada et al. (2009) interpret the results in the figure to reveal substantial differences in the conductivity-temperature ratios for the two regions. The authors state that the presence of considerably more water (as much as 1 wt%) in the western Pacific than in the European TZ is likely, assuming similar mineral and chemical compositions.

Shimizu et al. (2010b) continued this line of studies and imaged 3-D electrical conductivity distributions in and around the TZ beneath the North Pacific by inverting newly obtained geomagnetic responses at 13 observatories and cable responses of 8 submarine

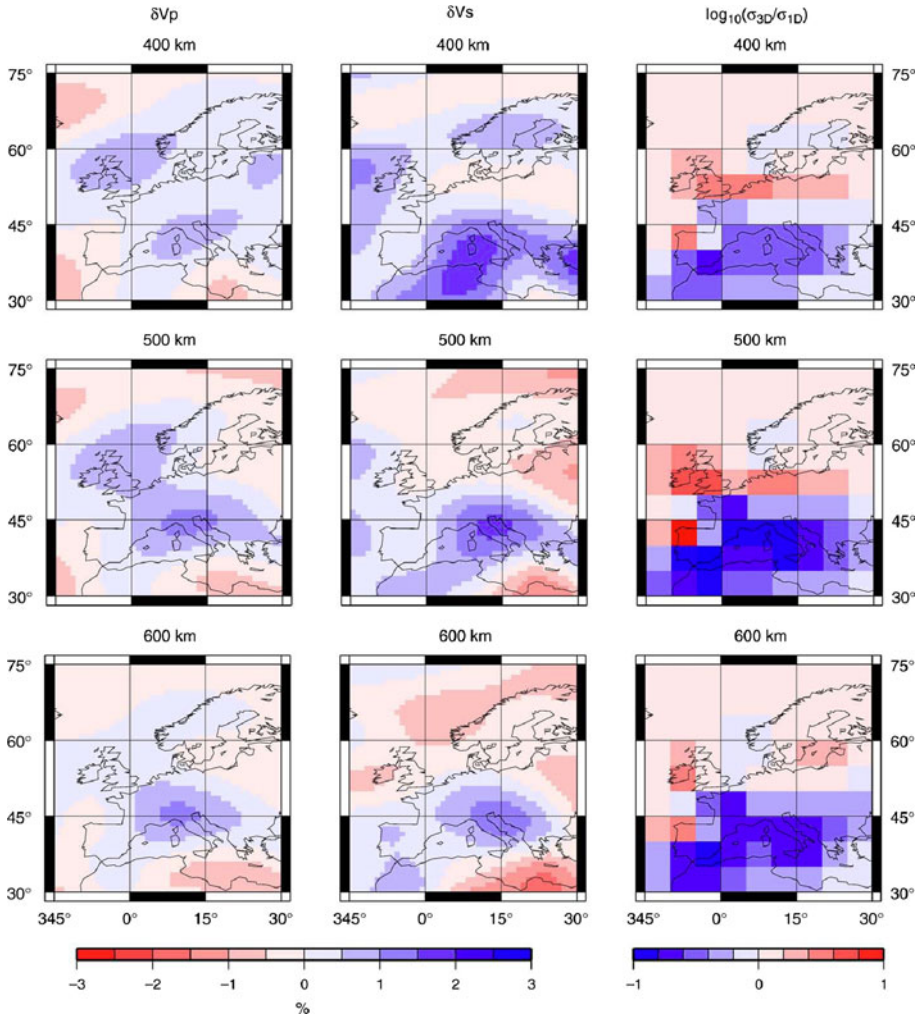

Fig. 8 Comparison of *P*- and *S*-wave tomography and results of 3-D EM inversion at depths of 400, 500, and 600 km. After Utada et al. (2009)

cables in the area. New responses were obtained from the longer time series compared with the studies of (Fukao et al. 2004; Koyama et al. 2006). The GDS responses at 9 periods from 5 to 35 days and MT cable responses at 9 periods from 1.7 to 10.5 were chosen to be used for the 3-D inversion for most of the geomagnetic stations and cables. Two new 1-D conductivity models beneath the North Pacific (with 2 and 3 jumps in the TZ) obtained by Shimizu et al. (2010a) were employed as reference models in this inversion. The grid spacing for the calculating forward problem was $2^\circ \times 2^\circ$ laterally and 50 km radially. The size of each block in the final inversion domain was $10^\circ \times 10^\circ$ laterally and 100 km radially, affording a total of $N = 19 \times 9 \times 5$ unknowns. Absolute values of the Laplacian of $\mathbf{m}$–$\mathbf{m}_0$ represented the regularization term in horizontal directions. No regularization of the model parameters in the vertical direction was applied. Their inversion required 8 iterations reducing the normalized misfit from 4.40 to 2.13.

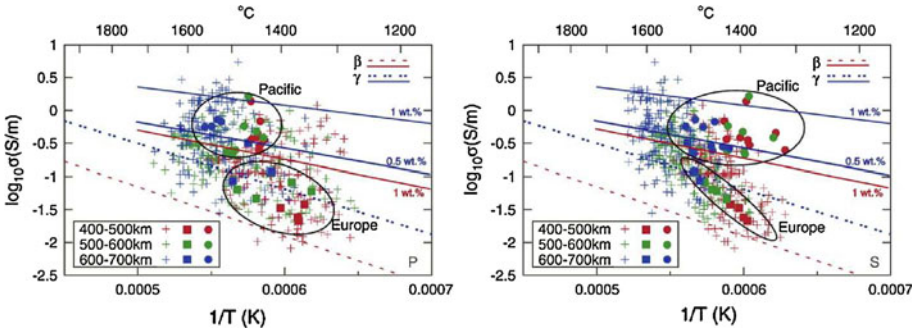

Fig. 9 Arrhenius relation between conductivity and converted temperature at depths of 400 (*red*), 500 (*green*), and 600 km (*blue*). Conductivity values are determined by 3-D EM inversion, and temperatures are converted from global *P*-wave (*left*) and *S*-wave (*right*) tomography. Plus and square symbols denote European results obtained with a spatial resolution of 5° × 5° and 15° × 15°, respectively. *Solid circles* denote the corresponding relations for the high-conductivity anomaly beneath the Philippine Sea (see Fig. 5). *Red dotted* (β) and *blue dashed* (γ) lines are those predicted from experimental data for dry wadsleyite and ringwoodite, while *red* and *blue solid lines* are those for water containing minerals (Yoshino et al. 2008), respectively. After Utada et al. (2009)

Figure 10 shows the resulting 3-D conductivity model. Note that the results are for the inversion run where a 1-D model with 3 jumps was used as reference model. The authors detected three features in the TZ: (a) a high conductivity anomaly beneath the Philippine Sea; (b) a high conductivity anomaly beneath the Hawaiian Islands, and (c) a low conductivity anomaly beneath and in the vicinity of northern Japan. The authors further noticed that the latter feature was not clearly seen in the model of Fukao et al. (2004). Shimizu et al. (2010b) also found the first feature to be in good agreement with the recent results of a regional sea floor study by Baba et al. (2010). The latter authors obtained and interpreted long-term ocean bottom EM data, and revealed that the conductivity in the upper mantle (down to TZ) is significantly higher beneath the Philippine Sea plate than that beneath the Pacific plate. Baba et al. (2010) also pointed out that a similar but weaker contrast can be seen in the TZ conductivity.

Shimizu et al. (2010b) interpreted their 3-D results in a similar way as done by Utada et al. (2009). Figure 11 shows the relationships between the converted temperature and electrical conductivity in the three regions mentioned above. From these relationships the authors concluded that the high conductivity beneath the Philippine Sea cannot be explained only by the temperature effect. If the cause of the high conductivity is due to the amount of water, the region requires more than 1 wt% in the TZ. As was already pointed out by Utada et al. (2009), the possible presence of water in the TZ may be a consequence of transportation of water by a subducting slab deep into the mantle beneath the Philippine Sea region.

The 3-D results discussed above deal with semi-global (or even more regional, as in Europe) inverse problem settings. Kelbert et al. (2008) developed a 3-D EM inversion scheme for the whole globe. Their scheme is based on non-linear conjugate gradients. To calculate responses and misfit gradients they generalized and extended an existing staggered-grid finite difference solver by Uyeshima and Schultz (2000). Using spherical harmonics in each inhomogeneous layer to parameterize the model space, they inverted a suite of synthetic data sets generated using checkerboard models to test the inversion and to study vertical and horizontal resolution of currently available data sets. The inversion was

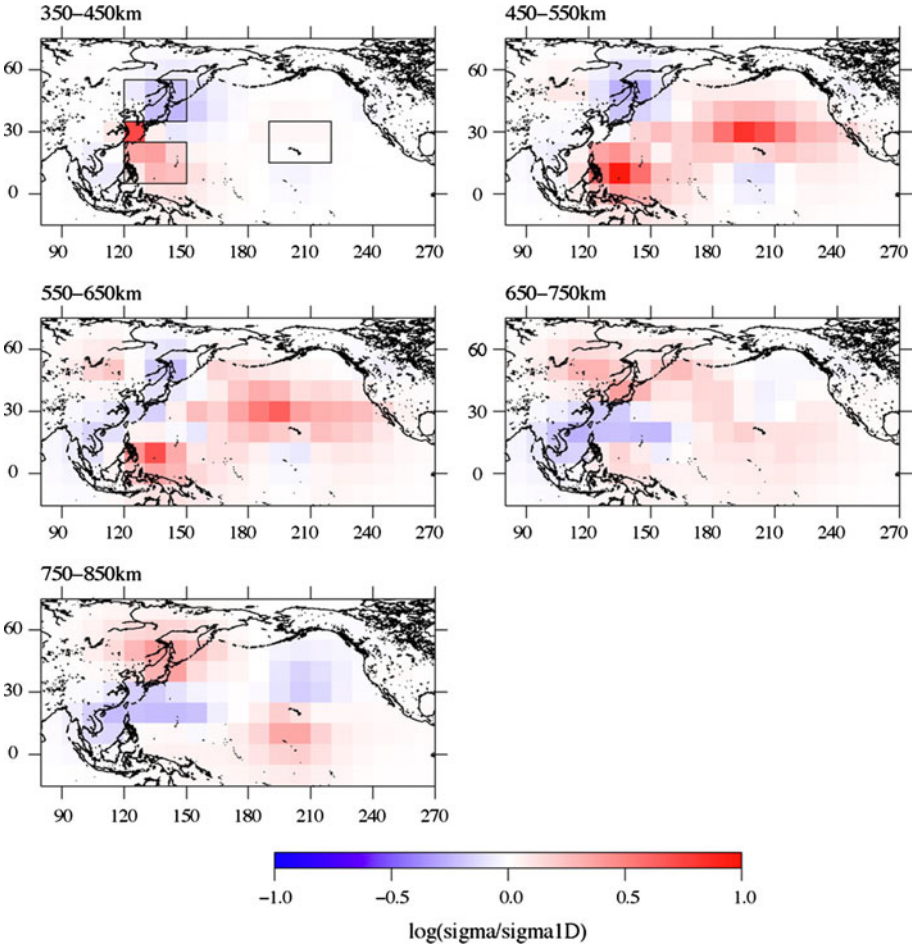

Fig. 10 3-D conductivity model beneath the North Pacific obtained by inverting the observed cable and GDS responses. *Boxes* in upper left plot depict the regions where the results are further analyzed (see Fig. 11). After Shimizu et al. (2010b)

regularized by minimizing deviations from the reference model, with a norm that penalized higher degree and order terms and jumps between layers.

Kelbert et al. (2008) concluded that responses in the period range 5–107 days resolve large scale (300–500 km vertically, and thousands of km horizontally) heterogeneities in mantle electrical conductivity reliably at the depth range 670–1,600 km. They also demonstrated that by extending induction responses to 0.2–5 days (assuming a dipole source), upper-mantle structure could also be resolved. However, as was stated earlier and also mentioned in their paper, interpreting data at these shorter periods is a challenging task, because source structure is much more complex and variable in time at these short periods.

Kelbert et al. (2009a) used the developed inversion scheme to obtain the first global 3-D model of mantle electrical conductivity. They parameterized the 3-D conductivity distribution at depths between the surface and 1,600 km by 8 spherical inhomogeneous layers of 100, 150, 160, 110, 150, 230, 300 and 400 km thickness, in each of which lateral

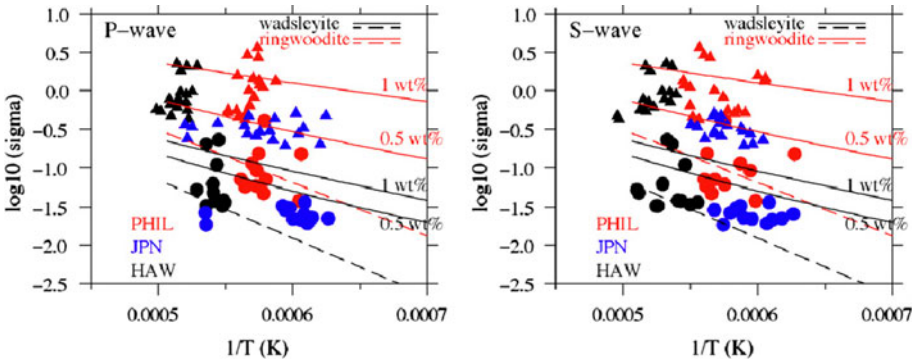

Fig. 11 The relationship between the converted temperature and electrical conductivity in three regions. The *red*, *blue* and *black* symbols indicate the region beneath the Philippine Sea (PHIL), northern Japan (JPN), and Hawaii (HAW), respectively. See Fig. 10 for the corresponding regions. *Solid circles* and *triangles* are for the conductivity and temperature in the depth ranges of 400–500 and 500–650 km, respectively. The *lines* show the experimental models for wadsleyite (*black*) and ringwoodite (*red*), respectively, obtained by Yoshino et al. (2008); the *dashed lines* are for the model under the dry condition, and the *solid lines* are for the hydrous minerals. After Shimizu et al. (2010b)

conductivity variations around the 1-D reference model of Kuvshinov and Olsen (2006) are parameterized by spherical harmonics up to degree and order 9. Conductivity jumps at 410, 520 and 670 km were allowed to mimic major mineral phase transitions in TZ. Below 1,600 km the layers were assumed to be homogeneous with a fixed conductivity value. They used a compilation of the *C*-responses at 59 observatories equator-ward of 60° geomagnetic latitude from the studies of Fujii and Schultz (2002; responses from 53 observatories) and Schultz and Larsen (1987; responses from 6 mid-latitude observatories).

Regarding the responses of Fujii and Schultz (2002) a comment is appropriate at this point. The authors discovered that the influence of the auroral current system is seen at surprisingly low geomagnetic latitudes, 40° and 50° for the vertical and northern components, respectively, resulting in a strong bias of GDS *C*-responses at high latitudes. To minimize artifacts due to this source they suggested a correction scheme based on a representation of an auroral source as an infinitesimally thin circular line current flowing at a height of 300 km, at 23° from the geomagnetic pole.

For inversion Kelbert et al. (2009a) used responses estimated at 28 periods from 5 to 106.7 days. The lateral grid for forward problem calculations was chosen as 10° × 10°. To account for the ocean effect the correction formula (19) was applied, where the predicted responses were calculated with the use of integral equation (IE) solver (cf. Kuvshinov 2008) using a much denser 1° × 1° grid. The regularization parameter was tuned to provide normalized misfit of 1.30.

Figure 12 (left panel) shows the results of Kelbert et al. (2009a). The authors note that in regions with poor data coverage, including most of Africa, South America, and the Indian and South Pacific Oceans, conductivity is poorly constrained at all depths. Their inversion suggests enhanced conductivity at TZ depths along the circum-Pacific margin extending from western North America, through the Aleutian arc and East Asia, and into the Indian Ocean and Australia. Most notably, higher conductivities are found beneath Japan, eastern China, and in the areas of the Izu-Bonin and Tonga slabs. The central Pacific basin is seen to be more than an order of magnitude more resistive than the surrounding conductive regions. High conductivities in and below TZ correlate with the present-day

distribution of cold, high velocity, subducted slabs (Fukao et al. 2001). It is remarked, that based on temperature alone, this cold subducted material should be relatively resistive (cf. Huang et al. 2005; Yoshino et al. 2008) and like Koyama et al. (2006) and Utada et al. (2009) is taken as indication that water, carried into transition zone with the subducting slabs, provides a plausible explanation for the enhanced conductivities.

Based on their global conductivity maps Kelbert et al. (2009a) estimated the water content of the TZ by comparing with laboratory electrical conductivity measurements of the main TZ minerals (wadsleyite and ringwoodite) of varying hydrogen content (cf. Huang et al. 2005; Yoshino et al. 2008; Karato and Dai 2009). Specifically they compared conductivity profiles from their 3-D inversion to those derived from the relation between conductivity and water content given by Yoshino et al. (2008) with water content varying from 0 to 1%. They showed that 0.5–1 wt% water might be required to achieve the highest conductivities (0. 5–2.0 S/m) in the lower transition zone, for example, beneath Japan. The more resistive areas (for example, central and southern Europe) are consistent with dry mantle conditions with no more than 0.1 wt%. This is in agreement with results obtained by Utada et al. (2009). In conclusion Kelbert et al. (2009a) remarked that the data set used in their study provides limited vertical and horizontal spatial resolution of the resulting model and they state that this set could be improved by augmenting the number of observatories.

More recently, Kelbert et al. (2009b) have obtained better quality estimates of GDS C-responses at more (118) mid-latitude ($<60^\circ$) observatories, in the extended (to shorter periods) period range (between 2.1 and 102.4 days). To estimate responses, hourly mean geomagnetic data for 10 years (1995–2004) of observations were used. The responses were corrected for the ocean effects in the same fashion as was done by Kelbert et al. (2009a). The correction for the auroral effects essentially followed (Fujii and Schultz 2002), but the amplitude, phase and height of the auroral ring current model were fit to the new data set period by period using a simple least squares-based procedure to achieve the best possible correction. Finally, 5 observatories that produced outliers due to obvious proximity to the magnetic dip equator were removed from the data set. The corrected responses were inverted in the same manner as in Kelbert et al. (2009a), using a degree and order 9 spherical harmonic parameterization and a $5^\circ \times 5^\circ$ modeling grid. Their best fit model (RMS $= 2.24$) is shown in the right panel in Fig. 12. It is seen that the new 3-D model significantly differs from the 3-D model obtained earlier (Kelbert et al. 2009a). This is especially true for the conductivity distributions in the southern hemisphere. The authors conclude that additional source complications are still present at the auroral latitudes. They also note that the new data set cannot be fit with the relatively coarse parameterization and discretization that were previously used. Smaller scale features and better understanding of the sources are clearly required to fit these data. Work is currently underway to obtain a finer model that would satisfy the data, as well as to improve on the source assumptions.

An alternative global 3-D frequency-domain inversion scheme has been proposed by Kuvshinov et al. (2008) (see also Chapter 2 of Kuvshinov et al. (2010)). Their optimization is based on a modern version of the QN method (cf. Nocedal and Wright 2006; limited memory QN (LMQN)), while the forward solver is based on an IE solution. It is well known that the efficiency of 3-D inversion depends critically on the ability to perform fast and robust calculations of the responses (forward prediction). Since their forward problem calculations are based on IE formulation, the most time-consuming part of the simulations (calculation of the tensor Green's functions) is performed only once, prior to the inversion. Modeling experiments demonstrated that isolating calculation of Green's functions

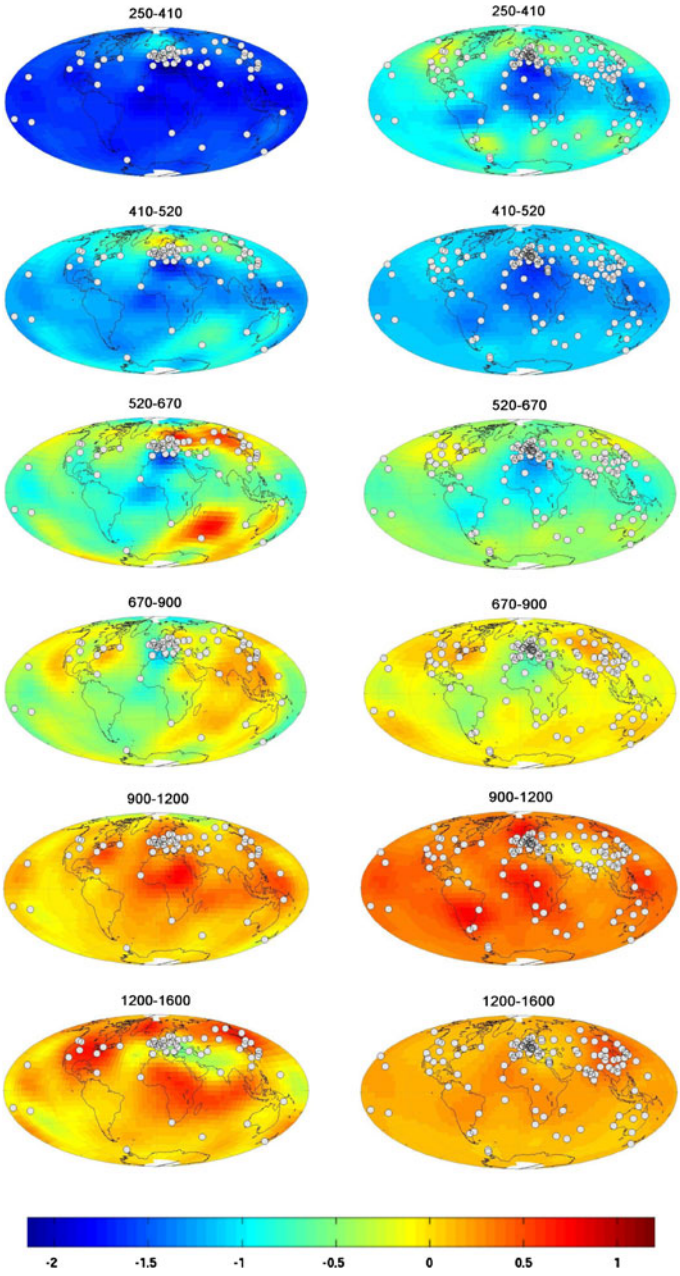

Fig. 12 *Left* global 3-D conductivity model obtained by Kelbert et al. (2009a) by inverting the GDS responses at 59 observatories. *Right* global 3-D conductivity obtained by Kelbert et al. (2009b) by inverting GDS responses at 114 observatories. Scale is in $\log_{10} \sigma$

accelerates by more than one order of magnitude the inverse solution. Further improvement in computation time stems from the parallelization of the IE solver. Since forward calculations are completely independent with respect to frequencies, they are performed at

different frequencies in parallel on N_f processors, where N_f is the number of analyzed periods.

Semenov and Kuvshinov (2010) used this inversion scheme to obtain an alternative global 3-D model of mantle conductivity. They estimated GDS *C*-responses at 133 mid-latitude observatories in the period range between 3.9 and 109.2 days using all available hourly mean geomagnetic data for 51 years of observations (1957–2007).

Recognizing that the influence of the auroral current system is seen in *C*-responses down to geomagnetic latitude of 40° *globally* (cf. Fujii and Schultz 2002). Semenov and Kuvshinov (2010) discovered that the auroral effect in *C*-responses reveals a strong longitudinal variability. It is known that the auroral effect is seen as the decay of the real parts of the responses towards the higher latitudes. The authors showed that the pattern of the decay varies with the region. Europe appears to be the region with lesser level of distortion. It is interesting that imaginary parts are almost unaffected by the auroral source, thus confirming the fact that in the considered period range induction is negligible for the small-scale pattern of the source (see Fig. 1 of this review and corresponding discussion in the text). Assuming: (a) the independence of the auroral signals on the Earth's conductivity (no induction); and (b) longitudinal variability of the auroral effect, Semenov and Kuvshinov (2010) developed an approximate scheme to account for this. In contrast to (Fujii and Schultz 2002) they do not correct the observed fields but assume that the predicted (during inversion) responses are contaminated by the auroral source. The level of longitudinally dependent contamination is estimated quantitatively on the basis of analysis of observed and predicted responses prior to inversion. To calculate the fields from an auroral source they used the same—as in (Fujii and Schultz 2002)—geometry of the source with the only difference that they assumed current flows at an altitude of 110 km.

For the 3-D inversion of their data set it was assumed that lateral heterogeneity is present in the depth range 410–1,600 km. Semenov and Kuvshinov (2010) parameterized the 3-D conductivity distribution in this depth range by 5 spherical inhomogeneous layers of 110, 150, 230, 300 and 400 km thickness. The layers were embedded into an a priori 1-D section very similar to that obtained by Kuvshinov and Olsen (2006). Above 410 km and below 1,600 km the layers were assumed to be homogeneous with a fixed conductivity. Forward problem calculations were done on a 3° × 3° grid. The lateral size of the blocks of the inversion domain was 9° × 9°, amounting to a total $N = 40 \times 20 \times 5$ unknowns. λ was chosen such that a normalized misfit of 1.09 was obtained; to reach this value required 25 iterations, with an initial misfit of 5.5.

Figure 13 compares the results of Semenov and Kuvshinov (2010) with the results of Kelbert et al. (2009b). The images differ in detail (for example, they differ in North America), but nonetheless reveal two robust features: (1) enhanced conductivity beneath Japan and eastern China; and (2) reduced conductivity beneath southern Europe and northern Africa. The latter is in agreement with the results of the semi-global study of Utada et al. (2009), while the enhanced conductivity in eastern China is in accord with the results of Ichiki et al. (2001). However, high conductivities beneath Japan and low conductivities beneath Hawaii contrast with the results of Shimizu et al. (2010b). The images of Semenov and Kuvshinov (2010) are seen to be patchier than those of Kelbert et al. (2010b). Most plausible reason for this seems to lie in the different parameterizations of the model—spherical harmonic coefficients in Kelbert et al. (2009a, b) and conductivities of the blocks in (Semenov and Kuvshinov 2010). Both inversions show enhanced conductivities in the polar regions. Most probably this is an artifact due to as yet insufficient account/correction for the auroral source effect.

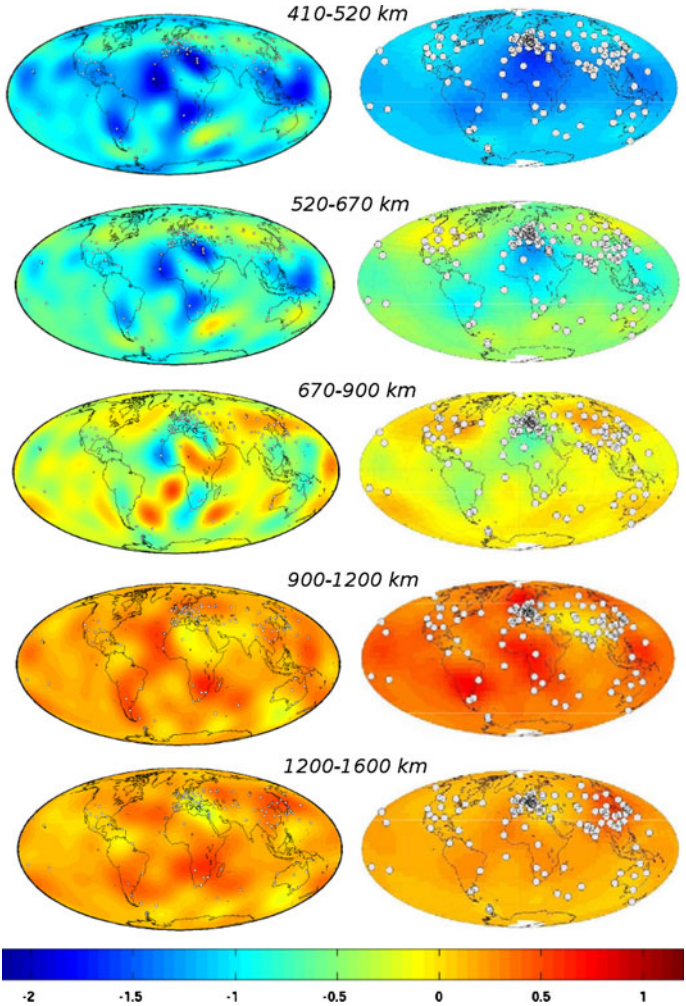

Fig. 13 *Left* global 3-D conductivity model (filtered up to degree $n = 10$) obtained by Semenov and Kuvshinov (2010) by inverting the GDS responses at 133 observatories. *Right* global 3-D conductivity obtained by Kelbert et al. (2009b) by inverting GDS responses at 114 observatories. Scale is in $\log_{10} \sigma$

2.5 Global 3-D Inversion in Time Domain

Tarits and Mandea (2010) developed a 3-D EM time-domain technique to invert 32 years (1958–1990) of magnetic monthly mean values from 120 geomagnetic observatories to image the conductivity in the middle mantle. Their interpretation scheme includes two steps. As a first step a source field model and an initial 1-D conductivity profile are determined. To determine a source they used a potential representation similar to that described by Eqs. 3–6 but written in the time domain. The authors obtained time series of external and internal coefficients up to degree $n = 3$ exploiting regularized least square method. A 1-D conductivity profile was then obtained by a regularized inversion of global C-responses. These responses (at a number of periods) have been converted from Q_1

responses (see Eq. 14) that were estimated by processing time series of internal and external coefficients associated with P_1^0 term. In the second step, actual 3-D inversion was performed based on minimization of the following penalty functional

$$\sum_{\mathbf{r}_a \in \text{Sites}} \sum_{t \in T} W_0(\mathbf{r}_a) D(\mathbf{r}_a, t) |\mathbf{B}(\mathbf{m}, t, \mathbf{r}_a) - \mathbf{B}^{\text{exp}}(t, \mathbf{r}_a)|^2 + \lambda \sum_{i,j} \left[\log(\sigma_i/\sigma_j)\right]^2. \quad (31)$$

Here $\mathbf{B}$ and $\mathbf{B}^{\text{exp}}$ are predicted and observed vector magnetic field, respectively, $D(t, \mathbf{r}_a)$ is the inverse of the squared uncertainties (taken as 1 nT). The weights W_0 ($\mathbf{r}_a$) were obtained using the formalism proposed by Mochizuki et al. (1997) to make the observatory distribution uniform on average. The sum is over all the observatories and all time steps. The regularization term is the sum squared of all the log-conductivity contrasts in the model. The subscripts i and j designate the conductivity value in either cell or layer i or j. The damping parameter is adjusted so that the damped regularization is smaller than the misfit. Their inversion technique minimizes (31) with a steepest descent algorithm adapted from the work of Beiner (1973). Forward 3-D time-domain predictions rely on the Fourier transform of the results of the 3-D frequency-domain solution, based on the spectral domain method (Tarits et al. 1992).

3-D inversion was initiated with a 1-D conductivity model obtained as a first step. The parameters for the inversion are the conductivity in the cells of the inversion grid. Only the layer between 900 and 1,400 km was assumed to be heterogeneous. Other layers were assumed to be homogeneous with conductivities fixed to their initial 1-D model. Tarits and Mandea (2010) used a 15° × 15° inversion (and forward) grid, thus estimating conductivity in 288 cells. Their results reveal (see Fig. 14) low conductivities beneath the Australian region, western Africa, near Japan, North and central America, and high conductivities in eastern Africa, South East Asia and Eurasia. When compared with the results of Kelbert et al. (2009b) and Semenov and Kuvshinov (2010) significant discrepancies can be observed. The most striking feature of the model by Tarits and Mandea (2010) model is that it shows much stronger conductivity contrast (about 2–3 decimal logarithmic units) than the other two models (less than 1 log unit).

3 Deep Induction Studies from Space

Olsen (1999b) in his review summarized the induction studies from space prior to the launch in 1999 of the Danish satellite Oersted which opened a new era of modern LEO geomagnetic satellite missions. Below we discuss recent advances in this field.

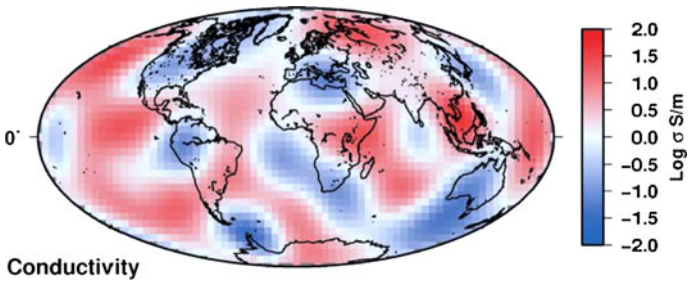

Fig. 14 Conductivity distribution between 900 and 1,400 km (filtered up to degree $n = 7$) obtained by Tarits and Mandea (2010). After Tarits and Mandea (2010)

To date all practical inversions of existing satellite data have been for 1-D (or at most of 2-D) conductivity models (cf. Constable and Constable 2004; Kuvshinov and Olsen 2006; Velimsky et al. 2006; Martinec and Velimsky 2009; Velimsky 2010). But even in the case of 1-D models such inversions are non-trivial, since LEO satellites typically move with speeds of 7–8 km/s and in reality measure a mixture of temporal and spatial changes of the geomagnetic field.

Satellite data are either analyzed in the time or frequency domain and differ in respects, although a number of fundamental assumptions and processing steps are similar.

First, in both methods a potential representation of the magnetic field is assumed at LEO satellite altitude. Second, both methods use signals originating from the magnetospheric ring current. Third, dipolar characteristics of this current are usually assumed. Therefore the spherical harmonic expansion is limited to external and internal terms of degree $n = 1$ and order $m = 0$ as a result of which the magnetic field potential can be approximated (in time domain) as

$$V = a\left[\hat{\varepsilon}_1^0(t)\left(\frac{r}{a}\right) + \hat{\imath}_1^0(t)\left(\frac{a}{r}\right)^2\right]P_1^0(\cos\vartheta_d), \tag{32}$$

where "hat" is used to distinguish coefficients in the time domain from the corresponding coefficients in the frequency domain (cf. Eq. 3). Concerning higher harmonics, Kuvshinov and Olsen (2006) noticed that including more zonal terms in the potential expansion did not improve their frequency-domain results appreciably. Analysis by Martinec and Velimsky (2009) also showed that the magnetic field energy at higher harmonic degrees is at least one order of magnitude smaller than the energy of the dipolar field. Moreover the difference rises to two orders of magnitude for periods longer than 10 days. It should be noticed that the effect of axial asymmetry of the magnetospheric ring current is well recognized (e. g. Olsen and Kuvshinov 2004; Balasis et al. 2004; Balasis and Egbert 2006) but so far is not considered in the inversions of existing satellite data.

As for common processing steps between time and frequency domain analyses, these are as follows: (a) isolation of the magnetospheric signals, $\delta\mathbf{B} = \mathbf{B} - \mathbf{B}_m$, by subtracting from satellite signals, $\mathbf{B}$, an appropriate model of static geomagnetic field and secular variation originating in the core, $\mathbf{B}_m$, over the period of analysis; models of Sabaka et al. (2004) or Olsen et al. (2009) are usually used for this aim; (b) analysis of night-side data only in order to minimize the contamination from Sq and equatorial electrojet currents; (c) ignoring data from high latitudes to suppress effects of auroral electrojets and field-aligned currents.

3.1 Frequency-Domain 1-D (and Quasi 1-D) Induction Studies

Constable and Constable (2004) processed 6 months of vector magnetic data collected by the Magsat mission (Magsat was operative during the November 1979–May 1980). From these data time series of external and internal coefficients, $\hat{\varepsilon}_1^0(t)$ and $\hat{\imath}_1^0(t)$ (cf. Eq. 32) were estimated, on a track by track basis (usual practice when analyzing single satellite data). In this case the sampling interval of the recovered time series is given by the orbit period (approximately 1.5 h). From these time series Q-responses (cf. Eq. 7) were estimated using a multi-taper approach (e.g., Riedel and Sidorenko 1995; Prieto et al. 2007) in the period range between 7 h and 100 days. Subsequently, Q-responses were transformed to C-responses (cf. Eq. 14). Finally, standard D^+ (Parker and Whaler 1981) and Occam's (Constable et al. 1987) inversions were applied to obtain a 1-D electrical conductivity

structure from the estimated C-responses. The authors found that a near-surface conductor of thickness less than 10 km is required, with a conductivity-thickness product almost exactly that of an average Earth ocean. Inversions suggested that an increase in conductivity at 440 km depth, predicted by recent laboratory measurements on high pressure phases of olivine, is not favored by the data, although, as in previous studies, the 670 km discontinuity between the TZ and lower mantle is associated with a two orders of magnitude jump in conductivity. A new feature in their inversion was a further increase in lower mantle conductivity up to 200 S/m or higher at a depth of 1,300 km.

Kuvshinov and Olsen (2006) estimated in a similar manner C-responses for periods ranging from 14 h to 4 months using five years (2001–2005) of simultaneous magnetic data collected by the three satellites Oersted, CHAMP and SAC-C.

The principal difference in estimation of $\hat{\varepsilon}_1^0(t)$ and $\hat{\imath}_1^0(t)$ compared with previous works is that they used another time parameterization since track by track basis is not suitable for the analysis of simultaneous data from more than one satellite due to lack of a common natural time basis (e.g., the satellites do not pass the equator simultaneously). This difficulty was overcome by parameterizing the time dependency of the coefficients by cubic B-splines (cf. Olsen et al. 2002). In their application the spacing of the spline knots was 4 h.

To estimate Q-responses Kuvshinov and Olsen (2006) used a section averaging approach similar to that employed by Olsen (1998). A regularized quasi-Newton algorithm (Byrd et al. 1995) was exploited to interpret the responses in terms of a 1-D mantle conductivity. For depths > 400 km the conductivity obtained from their C-responses is somewhat similar to that derived from ground-based data. All models generally show a monotonic increase of conductivity from 0.03 to 0.08 S/m at $z = 400$ km depth to 1–2 S/m at $z = 900$ km depth. However, conductivity based on their satellite responses is slightly (but systematically) higher at all depths below 400 km. For depths greater than 900 km the conductivities recovered from ground-based data and their satellite responses were almost constant, as opposed to the large conductivity increase reported by Constable and Constable (2004). However, Kuvshinov and Olsen (2006) questioned the result of Constable and Constable (2004) suggesting that their large increase in conductivity is an artifact due to the multi-taper approach in combination with the short Magsat time-series of only 6 months.

Kuvshinov and Olsen (2006) also stated that at periods shorter than 7 days their responses are most probably influenced by induction in the oceans. The authors corrected the data for the ocean effect using the following scheme

1. The external (inducing) field (i.e., time series of the expansion coefficient $\hat{\varepsilon}_1^0(t)$) is determined from $\delta\mathbf{B}$
2. Using this time–space structure of the external field, synthetic satellite magnetic signals for 1-D and 3-D conductivity models are predicted. The 3-D model consisted of a 1-D mantle conductivity, overlain by nonuniform ocean. Details of this magnetic field prediction, which is based upon a Fourier transformation of the inducing field and frequency domain forward modeling, is given in (Kuvshinov et al. 2006a).
3. Correcting the magnetic field residuals, δB, for induction in the oceans is done according to

$$\delta\mathbf{B}^{\mathrm{corr}} = \delta\mathbf{B} + \delta\mathbf{B}^{\mathrm{1D}} - \delta\mathbf{B}^{\mathrm{3D}}. \tag{33}$$

4. Recomputed $\hat{\varepsilon}_1^0(t)$ and $\hat{\imath}_1^0(t)$, Q- and C-responses, and finally 1-D conductivity profiles are obtained from the corrected residuals, $\delta\mathbf{B}^{\text{corr}}$.

Inversion of the corrected C-responses resulted in conductivities for depths shallower than 400 km that were more consistent with values derived from ground-based data, although the correction scheme did not produce reduction in misfit.

3.2 Time-Domain 1-D (and 2-D) Induction Studies

Velimsky et al. (2006) performed the first inversion of satellite (CHAMP) data directly in the time domain. In their study the authors assumed that the satellite travels in a nearly polar orbit and moves sufficiently fast compared to the time variation of the ring current. Data recorded during 11 storm events in 2001–2003 years were processed track by track, yielding time series of spherical harmonic coefficients. The two-step spherical harmonic analysis proposed by Martinec and McCreadie (2004) was applied allowing for determination of—on a track by track basis—the colatitude range where the data are free of polar disturbance. The 1-D inversion was performed by minimization of the following misfit functional

$$\phi_d(\mathbf{m}) = \frac{1}{N_I}\sum_{i\in I}\sum_{n=1}^{N_Z^i}\left|Z_n^{i,\text{exp}} - Z_n^{i,\text{pred}}(\mathbf{m})\right|^2. \tag{34}$$

Here I is a particular selection of N_I tracks, $Z_n^{i,\text{exp}}$ and $Z_n^{i,\text{pred}}(\mathbf{m})$ are observed and predicted spherical harmonic coefficients of the vertical component (of degree n and order 0), respectively, and N_Z^i is actual track-dependent truncation degree, which varied between 1 and 4. Vector of model parameters $\mathbf{m}$ was described by layer conductivities and depths of layer interfaces. In the inversion no constraints on smoothness of conductivity models were implemented and a full model space search of low dimension was used. The forward problem solver is based on a spherical harmonic finite element approach (cf. Velimsky and Martinec 2005) and is employed in all works by Velimsky and Martinec to be discussed below.

From their inversion Velimsky et al. (2006) concluded that: (1) in the upper 50 km their inversion solidly recovers a conductive layer corresponding to averaged surface conductance; (2) the conductivity of the lower mantle is established at 6 S/m assuming the upper–lower mantle interface is fixed at 670 km depth; (3) the satellite data favor models with a large jump around 1,000 km to unrealistically high conductivity values in excess of 10^3 S/m; (4) the resolution of the method in the resistive upper mantle sandwiched between conductive crust and lower mantle is poor. Nevertheless, an upper bound of 0.01 S/m is suggested by the data; (5) a conductivity increase in the transition zone is not observed. Overall, their study proved the feasibility of time-domain approach to deep induction studies.

Martinec and Velimsky (2009) (see also Martinec 2010) continued the efforts to interpret satellite data in the time domain. The authors developed an adjoint approach (analogous to that used in frequency domain studies) allowing for calculation of the gradient of the misfit (34) with respect to model parameters for the price of only one additional (backward in time) forward calculation irrespective of the number of conductivity parameters. Using this approach they applied conjugate gradient method to infer 1-D and 2-D conductivity structures of the Earth using 1 year (2001) of CHAMP data. Given the positions of layer interfaces the logarithms of resistivities for each layer were arranged

into a model vector **m**. As in (Velimsky et al. (2006)) analysis was performed on a track by track basis, with no regularization applied. They showed that a one year time series is capable of resolving both 1-D and 2-D structures in the upper mantle and the upper part of the lower mantle, while it is not sufficiently long to reliably resolve the conductivity structure in the lower part of the lower mantle. The results of their 2-D inversion are summarized in Fig. 15. From these results Martinec and Velimsky (2009) concluded that the mantle conductivity variations in the latitudinal direction reach about 20% of the mean value in upper mantle and about 4% in the upper part of the lower mantle.

Velimsky (2010) applied a time-domain inversion approach to 7 years (2001–2007) of CHAMP data with emphasis on constraining lower mantle conductivity. This stems from the recent discovery of new post-perovskite phase in the lowermost lower mantle (D'') by ab initio calculations and high-pressure and temperature experiments (Iitaka et al. 2004; Oganov and Ono 2004).

Time series of $\hat{\varepsilon}_1^0(t)$ and $\hat{\imath}_1^0(t)$ are reconstructed with a time step of 1 h. In contrast to Velimsky et al. (2006) and Martinec and Velimsky (2009), who used track-by-track analysis, an approach similar to that used by Kuvshinov and Olsen (2006) was exploited to complete time series. The 1-D inversion was performed by LMQN minimization of the following misfit functional

$$\phi_d(\mathbf{m}) = \frac{k}{t_L - t_F} \int_{t_F}^{t_L} \left(\frac{\hat{\imath}_1^0(\mathbf{m}, t) - \hat{\imath}_1^{0,\exp}(t)}{\delta \hat{\imath}_1^{0,\exp}(t)} \right)^2 dt, \tag{35}$$

where k is a constant. A regularization term is also implemented and was defined as the L_2 norm of radial dimensionless Laplacian of the logarithm of resistivity, integrated over and then normalized by Earth's volume. The inversion of the recovered time series of internal coefficient, $\hat{\imath}_1^0(t)$, suggested lower mantle conductivities below 2 S/m, with an increase to 10 S/m in the D''. Values in the range 10–300 S/m, such as those obtained experimentally

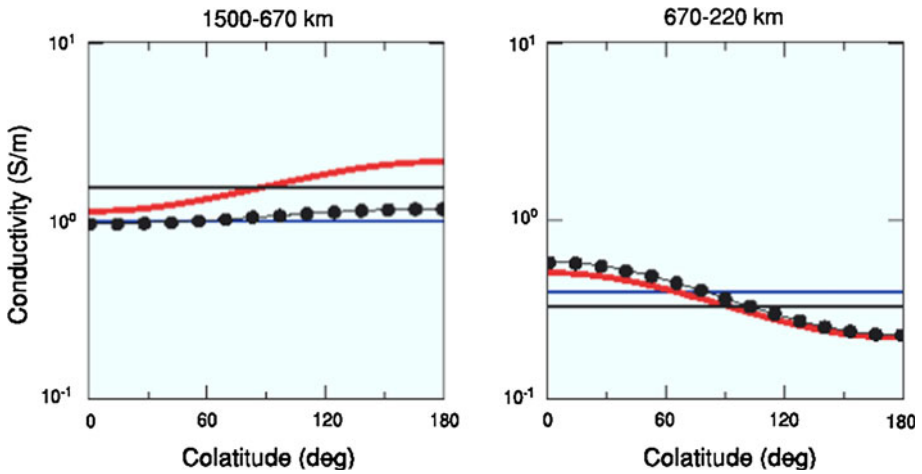

Fig. 15 Two-layer, latitudinally dependent conductivity model of the upper part of the lower mantle and the upper mantle (*left* and *right* panels). The model best fitting the 2001 CHAMP data (*red lines*), the starting model for the CG minimization (*blue lines*) and the model after the first iteration (*dotted line*) are compared to the best 1-D conductivity model. After Martinec and Velimsky (2009)

for post-perovskite by Ohta et al. (2008) were found to yield a slightly higher data misfit. Velimsky (2010), however, warns that the sensitivity of the data to the conductivity structure below 2,000 km is significantly reduced. Note that the lower mantle conductivity of Velimsky (2010) is in agreement with the estimate of the mean mantle conductivity obtained by Alexandrescu Mandea et al. (1999) and deduced from the study of the diffusion of impulses related to the geomagnetic secular variations (jerks) through the mantle.

3.3 Frequency-Domain 3-D Induction Studies

The forthcoming multi-satellite mission *Swarm* has initiated efforts to develop interpretational schemes to map 3-D mantle conductivity from space. In this subsection frequency-domain approaches are discussed; time-domain approaches will be discussed in Sect. 3.4. Note that so far no attempts have been made, using either approaches, to invert real satellite data in a 3-D frame.

One of the initial ideas was to use the local *C*-response formalism to interpret satellite data. It was shown by Kuvshinov et al. (2006a), by using results of end-to-end simulations (Olsen et al. 2006), that local *C*-responses can be procured from magnetic observations taken by the *Swarm* constellation. The necessary condition for such a retrieval is the determination of time series of external (inducing) and internal (induced) spherical harmonic expansion (SHE) coefficients of the magnetic potential that describe the magnetospheric source. These time series are assumed to be available as *Swarm* output product of the comprehensive modeling (cf. Sabaka et al. 2004; Olsen et al. 2007) which aims to separate magnetic contributions from various sources (originating in the core, lithosphere, ionosphere, and magnetosphere) in a form of corresponding SHE coefficients. From these coefficients, time series of magnetic field components can be synthesized on a regular (virtual) spatial grid and satellite *C*-responses on this grid can be determined by means of signal processing of the corresponding time series. But, in contrast to ground-based *C*-responses which have been obtaining from time series of directly observed field variations, satellite *C*-responses are synthesized from the time series of external and internal SHE coefficients. Their proper interpretation is, however, challenging.

Kuvshinov et al. (2009) discussed an approach based on an inversion of alternative transfer functions (elements of the *Q*-matrix) that connect external and internal potential coefficients. In the general case of a 3-D conductivity structure each external coefficient $\varepsilon_n^m(\omega)$ induces a whole spectrum of internal coefficients

$$\imath_k^l(\omega) = \sum_{n,m} Q_{kn}^{lm}(\omega)\varepsilon_n^m(\omega), \tag{36}$$

in which case the representation (8) for the potential (valid for a 1-D conductivity profile) transforms to

$$V = a\sum_{n,m}\varepsilon_n^m(\omega)\left[\left(\frac{r}{a}\right)^n Y_n^m + \sum_{k,l} Q_{kn}^{lm}(\omega)\left(\frac{a}{r}\right)^{k+1} Y_k^l\right]. \tag{37}$$

The misfit term for these transfer functions looks as (cf. Eq. 23)

$$\phi_d = \sum_{\omega\in\Omega}\sum_{n,m}\sum_{k,l} D_{kn}^{lm}(\omega)\cdot\left|Q_{kn}^{lm}(\mathbf{m},\omega) - Q_{kn}^{lm,\exp}(\omega)\right|^2, \tag{38}$$

where Q_{kn}^{lm} and $Q_{kn}^{lm,\exp}$ are predicted and observed elements of Q-matrix, respectively, $D_{kn}^{lm}(\omega)$ are the inverse components of the squared uncertainties of $Q_{kn}^{lm,\exp}$.

Observed elements, $Q_{kn}^{lm,\exp}$, are assumed to be obtained as follows. Based on results of end-to-end simulations it is expected that geomagnetic signals from the *Swarm* constellation will permit recovering time series of: (a) external coefficients up to degree $N_e = 3$ and order 1 and (b) internal coefficients up to degree $N_i = 9$. With the recovered time series in hand one can estimate $Q_{kn}^{lm,\exp}$ from the relation (36) using multivariate analysis (e.g., Bendat and Piersol 1968).

The advantage of working with Q-matrix is that the inversion setting does not depend on the source. However, this merit is counterbalanced by the necessity to perform a multivariate signal analysis which is non-trivial, especially bearing in mind that magnetospheric source is dominated by the $n = 1$, $m = 0$ term. To avoid this difficulty the authors also considered an alternative inverse problem formulation where the time spectra of the internal coefficients are analyzed instead. In that case the data misfit term is

$$\phi_d = \sum_{\omega\in\Omega}\sum_{k,l} D_k^l(\omega)\cdot\left|\imath_k^l(\mathbf{m},\omega) - \imath_k^{l,\exp}(\omega)\right|^2, \tag{39}$$

where $D_k^l(\omega)$ is the inverse of the squared uncertainties of $\imath_k^{l,\exp}(\omega)$. To minimize (22), with the data misfit in the form of (39) they applied the LMQN method. As forward modeling engine to calculate the data misfit gradient as well as the internal coefficients themselves they used their IE solver. In order to make 3-D inversion of $Q_{kn}^{lm,\exp}(\omega)$ or $\imath_k^{l,\exp}$ tractable Kuvshinov et al. (2009) developed an adjoint method for the efficient calculation of gradients of data misfit in the forms of Eqs. 38 and 39. They also presented the first results on verification of a 3-D inversion scheme based on analysis of $\imath_k^l(\omega)$. Later Kuvshinov et al. (2010; Chapter 8) provided more benchmarking exercises aimed at comparing the performances of this and alternative 3-D time-domain inverse solution (see Sect. 3.4), on two—smooth checkerboard and blocky—models.

As a final remark on this section we would like to mention that Pascal Tarits has also developed a 3-D inversion scheme based on analysis of Fourier spectra of internal spherical harmonic coefficients (cf. Chapter 4 of Kuvshinov et al. (2010)). His optimization procedure exploits a downhill simplex method, while the forward problem solver relies on the generalized spherical harmonic expansion (cf. Tarits et al. 1992).

3.4 3-D Time-Domain Induction Studies

Jakub Velimsky has developed an approach which is based on a time-domain setting and deals with a 3-D inversion of time series of internal coefficients (cf. Chapter 3 of Kuvshinov et al. (2010)). The misfit functional is similar to that described by Eq. 35, but includes summation over all internal coefficients. For the efficient calculation of misfit gradients Velimsky developed an adjoint approach similar to that developed by Martinec and Velimsky (2009). As Kelbert et al. (2008, 2009a, b) do, Velimsky uses spherical harmonics in each inhomogeneous layer to parameterize the model space. His optimization scheme exploits the LMQN method, while the regularization term is defined as in (Velimsky 2010). This 3-D time-domain inverse solver has been tested on a number of models and produced results of similar quality compared with the results from frequency-domain solver of Kuvshinov et al. (2009).

4 Conclusions

The results of the deep EM studies reviewed here reveal a substantial level of lateral heterogeneity in the upper and mid-lower mantle (down to depths of 1,500 km). Conductivity values vary laterally by more than one order of magnitude between resistive and conductive regions. As expected the overall tendency is that conductivity lateral variations diminish in magnitude with depth.

The family of 3-D conductivity distributions produced to date has yet to reach a consensus—different groups using different data sets or inverse methods obtain disparate results, complicating quantitative comparison with seismic tomography and geodynamic models. The present discrepancy is most probably due to: (a) inherent strong non-uniqueness of the inverse problem arising from spatial sparsity and irregularity of data distribution, variable data quality and limited period range; (b) very different inversion settings, including forward and inverse problem gridding, model parameterization, a priori information used, form of regularization term employed, and choice of damping parameter; (c) shortcomings of data analysis; (d) inconsistency of external field models, for example improper account/correction for the auroral effect and/or ignoring asymmetric part of the ring current; (e) possible inaccuracy in forward and inverse solutions.

5 Outlook

5.1 Extending Long-Term Magnetic (Geoelectric) Observations

While satellites are very important and perhaps indispensable, we believe the major input for 3-D conductivity studies will come from a reliable ground network of geomagnetic observatories. In spite of continuing efforts there are still major gaps in the ground station network, especially in oceanic areas and in the southern hemisphere. In the last decade a number of geomagnetic observatory projects have been initiated to improve the coverage by long-term measurements in those regions. From 2007 GFZ (Helmholtz-Zentrum Potsdam) operates geomagnetic observatory in South Atlantic Ocean on *St. Helene* Island (Korte et al. 2009). In 2008, a new observatory on *Easter* Island (South Pacific Ocean) was installed by Institute de Physique du Globe de Paris (France) and Direccion Meteorologica de Chile (Chulliat et al. 2009). Since 2009 National Space Institute at the Technical University of Denmark runs observatory on *Tristan da Cuhna* Island also located in South Atlantic Ocean (Matzka et al. 2009). The Institute of Geophysics, ETH Zurich (Switzerland) is on the way to install and run two geomagnetic observatories in the Indian Ocean—on *Gan* island, Maldives (in cooperation with Maldives Meteorological Service and National Geophysical Research Institute, Hyderabad, India), and on *Cocos* Island (in cooperation with Geoscience Australia).

A few long-term geomagnetic stations have been installed by Ocean Hemisphere Research Center (OHRC) of ERI (Shimizu and Utada 1999) in the Pacific Ocean within Ocean Hemisphere Network Project (1996–2000). Five stations at *Majuro* (Marshall Islands), *Pohnpei* (Micronesia), *Muntinlupa* (Philippines), *Atele* (Tonga), *Marcus* Island (Japan) are still running and OHRC plans to continue observations at these sites as long as possible.

The biased distribution of the land/island geomagnetic observatories is now at a stage of improvement by extending the geomagnetic observatories to the seafloor. Toh et al. (2004,

2006, 2010) reported successful running of two long-term seafloor geomagnetic stations. One station (called NWP) operates in the *North West Pacific* since 2001 and another station (called WPB) operates in the *West Philippine Basin* since 2006. Their seafloor data consist of the geomagnetic vector and scalar field measurements along with attitude measurements for both orientation and tilt. In addition horizontal components of the electric field are measured, thus allowing in principle (provided long enough time series of the EM field) for long-period magnetotelluric (MT) sounding.

Note that long period electric field measurements more and more often complement magnetic field observations. During 2001–2003 the MT data have been collected in the frame of Central Europe Mantle geoElectrical Structure (CEMES) project at positions of 11 permanent geomagnetic observatories situated within few 100 km along the South West margin of the East European Craton (cf. Semenov et al. 2008). Five years or longer MT measurements has been conducting in the frame of the EMScope component of the NSF Earthscope project. This experiment resulted in deployment of 7 backbone long-period MT stations across North America (Schultz 2010).

5.2 Use of Sq Signals

All 3-D inversions discussed in the paper deal with the *Dst* signals of magnetospheric origin resulting in conductivity distributions at depth greater than 400 km. Surprisingly, no studies have been conducted so far that invert Sq data in the frame of 3-D models. The advantage of inverting Sq signals is that it permits resolving conductivity structures at depths shallower than 400 km. Another advantage is that more Sq data are available for use in comparison to "magnetospheric" data. Since Sq signals are periodic (daily) variations, one can in principle work with Sq data on a single-day basis, in which case it is possible to use—along with the data from the global net of geomagnetic observatories—data from regional EM surveys for the same time period. A good example of such a survey is the AWACS experiment, within which an array of 57 instruments were distributed regularly across Australian continent and continuously measured the magnetic field during 1 year (1991) (cf. Chamalaun and Barton 1993), providing data in the otherwise gappy southern hemisphere. Another good example of a regional survey is the sea floor MT experiment in the Philippine Sea (cf. Baba et al. 2010) which provided data from 21 sites in the ocean region. It is interesting that for MT analysis Sq variations are usually considered as a source of noise and as a rule are filtered out before further MT analysis.

However, work with Sq data has its own shortcomings, which is most probably the reason why these signals have not been used in deep 3-D EM studies. The ionospheric source of Sq variations has a much more complex spatial geometry compared with magnetospheric source. Due to the strong spatial irregularity of the geomagnetic observations the determination of sources of Sq is non-trivial. One possibility is to perform spherical analysis of magnetically quiet days (when the geometry of Sq source is relatively simple) as was done, for example, by Schmucker (1999a, b). In addition the complexity of the Sq source and spatial irregularity of the observations rules out the possibility to use (on a global scale) traditional approaches of data analysis based on the *C*-response concept either in HGS or GDS + HGS versions. An obvious solution here is the analysis of the fields (or their Fourier spectra) themselves rather than responses as was done, for example, in (Kuvshinov et al. 1999) where global estimate of lithospheric resistivity was obtained by analyzing time spectra of vertical Sq components from 12 coastal observatories. Similar treatment of Sq signals is also discussed by Kuvshinov et al. (2007) and Kuvshinov and Utada (2010).

Concerning analysis of satellite Sq data one might remark that in contrast to signals originating from the magnetospheric current, it is not possible to recover the mantle conductivity distribution using satellite Sq data alone. The reason for this is that LEO satellites fly above the Sq source, and thus the Sq signals at satellite altitude are seen as being of purely internal origin. Thus there is no way to separate Sq fields in external and internal parts using only satellite data.

5.3 Use of Tidal Signals

Along with time-varying magnetic fields of magnetospheric and/or ionospheric origin, there exists another source of time-varying EM signals—electric currents induced by oceanic tides. As electrically conducting salt water moves through the ambient magnetic field of the Earth, it generates secondary magnetic and electric fields. These signals that can be detected either at sea floor or at coasts, have a potential to be used for deep EM sounding of the Earth. Actually the idea of using tidal signals for deep EM soundings is not new, but so far it was used only for quasi 1-D interpretation of electric field data (cf. Kuvshinov et al. 2006b). The advantage of working with tidal signals is twofold: (a) the geometry of tidal sources is known more accurately (cf. Erofeeva and Egbert 2002) than the geometry of ionospheric or/and magnetospheric sources; (b) sea floor magnetic fields from tidal sources contain substantial toroidal mode which is sensitive to resistive layers (for example lithosphere) of the Earth. The drawbacks are also rather evident: (a) in contrast to *global* ionospheric/magnetospheric sources the tidal source is confined only to oceanic regions; (b) due to the geometry of generating electric current which is governed by vertical component of the main magnetic field the tidal magnetic (and electric) signals are rather small in the vicinity of dip equator and unlikely can be used in this region; (c) seemingly the signals from only two tides—semi-diurnal M2 and diurnal O1—can be reliably extracted from the data thus limiting resolution in radial direction; (d) it is not simple to distinguish these signals from stronger Sq signal which is described by close frequencies; (e) one cannot use approaches based on the response concept. But nevertheless use of tidal signals for the Earth's probing in the frame of 3-D models seems worthwhile to implement.

5.4 Joint Analysis of Satellite and Ground-Based Data

The results of end-to-end model studies (see Chapter 6 of Kuvshinov et al. (2010)) indicate that it is difficult to determine time series of internal coefficients of relatively high degree and order (n, $m = 5$) even using data from forthcoming, the most advanced geomagnetic constellation mission, *Swarm*. Authors argue that joint analysis of satellite and ground-based (observatory) data is expected to improve the recovery of the internal, induced coefficients, and thereby enhance the capability to detect lateral conductivity variations.

5.5 Benchmarking of Independent 3-D Forward and Inverse Solutions

As reviewed here a number of 3-D forward and inverse solutions have been developed and implemented over the past years covering time and frequency domains. These approaches need to be robustly and systematically validated against each other. Such an intercomparison would help to resolve possible inaccuracy of independent forward and/or inverse solutions.

5.6 Proper Account/Correction for the Auroral Effect

Recent attempts to account/correct for the auroral effect (cf. Fujii and Schultz 2002; Kelbert et al. 2009a, b; Semenov and Kuvshinov 2010) in 3-D inversion of ground-based *C*-responses cannot be said to be fully successful. Artifacts are still present in global 3-D conductivity images at polar latitudes. A future goal, albeit challenging, would be to understand the physical processes occurring in the auroral regions in order to obtain quantitative models of the polar electrojets and incorporate these into global 3-D EM inversion schemes.

5.7 Refining Laboratory Electrical Conductivity Measurements

The discrepancy that currently exists between laboratory measurements of the electrical conductivity of the hydrous wadsleyite and ringwoodite is such that it effectively precludes drawing any firm conclusions about the water content in TZ. The controversy is not likely to be settled until more measurements by either group (Yoshino and coworkers, and Karato and coworkers) or preferably a third party have been obtained.

5.8 New Methods of Analysis of Ground-Based Data

There is still strong need for the methodologies that allow for working in unified and consistent manner: (a) with 3-D conductivity models of the Earth; (b) with arbitrary sources and thus in the whole period range under consideration; (c) with the data that are irregularly distributed on a globe. One promising (frequency domain) approach has been proposed in (Fainberg et al. 1990). Two basic ideas behind the method are: (a) one has to work with the fields (more exactly with the time spectra of the fields) rather than with the responses; (b) one has to determine simultaneously the parameters describing the source and conductivity distribution in the Earth. With the ultimate goal to work with the 3-D conductivity models, this method has been so far applied to estimate 1-D conductivity distribution in the middle and lower mantle (Singer et al. 1993). Obviously this approach can be also adapted for time domain setting. Probably the time domain version of this methodology is even more attractive for the implementation.

Acknowledgments I would like to thank the organizing committee of the 20th international workshop on Electromagnetic Induction in the Earth in Giza, Egypt for the invitation to present this review. I also thank Amir Khan for overall comments as well as help with improving the English presentation of this review. I am very grateful to all those who contributed material for this paper, in alphabetical order (K. Baba, A. Kelbert, A. Khan, Z. Martinec, J. Matzka, K.Ohta, N. Olsen, A. Schultz, A. Semenov, V. Semenov, H. Shimizu, P. Tarits, H. Utada, J. Velimsky) and I apologize to those whose material I could not include. This work has been supported in part by European Space Agency through ESTEC contracts No. 20944/07/NL/JA and No. 22656/09/NL/FF, and by the Russian Foundation for Basic Research under grant No. 09-05-01071-a.

References

Alexandrescu Mandea M, Gilbert D, Le Mouel J-L, Hulot G, Saracco G (1999) An estimate of average lower mantle conductivity by wavelet analysis of geomagnetic jerks. J Geophys Res 104(B8): 17735–17745

Baba K, Utada H, Goto T, Kasaya T, Shimizu H, Tada N (2010) Electrical conductivity imaging of the Philippine Sea upper mantle using seafloor magnetotelluric data. Phys Earth Planet Int. doi:10.1016/j.pepi.2010.09.010

Balasis G, Egbert GD (2006) Empirical orthogonal function analysis of magnetic observatory data: Further evidence for non-axisymmetric magnetospheric sources for satellite induction studies. Geophys Res Lett 33:L11311. doi:10.1029/2006GL025721
Balasis G, Egbert GD, Maus S (2004) Local time effects in satellite estimates of electromagnetic induction transfer functions. Geophys Res Lett 31:L16610. doi:10.1029/2004GL020147
Banks R (1969) Geomagnetic variations and the electrical conductivity of the upper mantle. Geophys J R Astr Soc 17:457–487
Becker TW, Boschi L (2002) A comparison of tomographic and geodynamic mantle models. Geochem Geophys Geosyst 3:1003. doi:10.1029/2001GC000168
Beiner J (1973) Analysis in phases of diffusion PI-C-12 beneath 300 MEV. Nucl Phys B53:349–365
Bendat J, Piersol A (1968) Random data: analysis and measurement procedure. Wiley, New York
Bercovici D, Karato SI (2003) Whole-mantle convection and the transition-zone water filter. Nature 425:39–44
Byrd R, Lu P, Nocedal J, Zhu C (1995) A limited memory algorithm for bound constrained optimization. SIAM J Sci Comput 5:1190–1208
Chamalaun FH, Barton CE (1993) Electromagnetic induction in the Australian crust: results from the Australia-wide array of geomagnetic stations. Explor Geophys 24:179–186
Chapman S, Price A (1930) The electric and magnetic state of the interior of the Earth as inferred from terrestrial magnetic variations. Phil Trans R Soc Lond A 229:427–460
Chulliat A, Lalanne X, Gaya-Pique LR, Truong F, Savary J (2009) The new Eastre Island magnetic observatory. In: Love JJ (ed) Proceedings of the XIIIth IAGA workshop on geomagnetic observatory instruments, data acquisition and processing. US Geological Survey Open-File Report 20091226, pp 47–53
Constable S, Constable C (2004) Observing geomagnetic induction in magnetic satellite measurements and associated implications for mantle conductivity. Geochem Geophys Geosyst 5:Q01006. doi:10.1029/2003GC000634
Constable S, Parker RL, Constable C (1987) Occam's inversion: a practical algorithm for generating smooth models from electromagnetic sounding data. Geophysics 52:289–300
Egbert G, Booker JR, Schultz A (1992) Very long period magnetotellurics at Tucson observatory: estimation of impedances. J Geophys Res 97:15113–15128
Erofeeva S, Egbert G (2002) Efficient inverse modeling of barotropic ocean tides. J Ocean Atmos Technol 19:183–204
Faccena C, Jolivet L, Piromallo C, Morelli A (2003) Subduction and the depth of convection in the Mediterranean mantle. J Geophys Res 108(B2):2099
Fainberg E, Kuvshinov A, Mishina L, Singer B (1990) The new approach to global deep soundings. Pure Appl Geophys 134:527–531
Fujii I, Schultz A (2002) The 3D electromagnetic response of the Earth to ring current and auroral oval excitation. Geophys J Int 151:689–709
Fukao Y, Widiyantoro S, Obayashi M (2001) Stagnant slabs in the upper and lower mantle transition region. Rev Geophys 39:291–323
Fukao Y, To A, Obayashi M (2003) Whole mantle P-wave tomography using P and PP-P data. J Geophys Res 108(B1):2021. doi:10.1029/2001JB000989
Fukao Y, Koyama T, Obayashi M, Utada H (2004) Trans-Pacific temperature field in the mantle transition region derived from seismic and electromagnetic tomography. Earth Planet Sci Lett 217:425–434
Haber E, Ascher UM, Oldenburg DW (2004) Inversion of 3D electromagnetic data in frequency and time domain using an inexact all-at-once approach. Geophysics 69:1216–1228
Hae R, Ohtani E, Kubo T, Koyama T, Utada H (2006) Hydrogen diffusivity in wadsleyite and water distribution in the mantle transition zone. Earth Planet Sci Lett 243:141–148
Huang XG, Xu YS, Karato SI (2005) Water content in the transition zone from electrical conductivity of wadsleyite and ringwoodite. Nature 434:746–749
Ichiki M, Uyeshima M, Utada U, Guoze Z, Ji T, Mingzhi M (2001) Upper mantle conductivity structure of the back-arc region beneath northeastern China. Geophys Res Lett 28:3773–3776
Iitaka T, Hirose K, Kawamura K, Murakami M (2004) The elasticity of the MgSiO3 postperovskite phase in the Earths lowermost mantle. Nature 430:442–445
Inoue T, Yurimoto H, Kudoh Y (1995) Hydrous modified spinel, Mg1.75SiH0.5O4: a new water reservoir in the mantle transition zone. Geophys Res Lett 22:117–120
Ito E, Katsura T (1989) A temperature profile of the mantle transition zone. Geophys Res Lett 16:425–428
Jiracek GR (1990) Near-surface and topographic distortions in electromagnetic induction. Surv Geophys 11:163–203
Karato S (1990) The role of hydrogen in the electrical conductivity of the upper mantle. Nature 347:272–273

Karato S (1993) Importance of anelasticity in the interpretation of seismic tomography. Geophys Res Lett 20:1623–1626
Karato S (2006) Remote sensing of hydrogen in Earth's mantle. Rev Miner Geochem 62:343
Karato S, Dai LD (2009) Comments on "Electrical conductivity of wadsleyite as a function of temperature and water content" by Manthilake et al. Phys Earth Planet Interiors 174:19–21
Kelbert A, Egbert G, Schultz A (2008) Non-linear conjugate gradient inversion for global EM induction: resolution studies. Geophys J Int 173:365–381
Kelbert A, Schultz A, Egbert G (2009a) Global electromagnetic induction constraints on transition-zone water content variations. Nature 460:1003–1007
Kelbert A, Egbert G, Schultz A (2009b) Spatial variability of mantle transition zone water content: evidence from global electromagnetic induction data. Abstracts of AGU Fall Meeting, San-Francisco
Kennett B, Engdahl E (1991) Traveltimes for global earthquake location and phase identification. Geophys J Int 105:429–465
Khan A, Connolly JAD, Olsen N (2006) Constraining the composition and thermal state of the mantle beneath Europe from inversion of long-period electromagnetic sounding data. J Geophys Res 111:B10102. doi:10.1029/2006JB004270
Khan A, Boschi L, Connolly JAD (2009) On mantle chemical and thermal heterogeneities and anisotropy as mapped by inversion of global surface wave data. J Geophys Res 114:B09305. doi:10.1029/2009JB006399
Khan A, Kuvshinov A, Semenov A (2010) On the heterogeneous electrical conductivity structure of the Earth's mantle with implications for transition zone water content. J Geophys Res 116:B01103. doi:10.1029/2010JB007458
Korte M, Mandea M, Linthe HJ, Hemshorn A, Kotze P, Ricaldi E (2009) New geomagnetic field observations in the South Atlantic Anomaly region. Ann Geophys 52:65–82
Koyama T (2001) A study on the electrical conductivity of the mantle by voltage measurements of submarine cables. PhD thesis, University of Tokyo
Koyama T, Shimizu H, Utada H, Ichiki M, Ohtani E, Hae R (2006) Water content in the mantle transition zone beneath the North Pacific derived from the electrical conductivity anomaly. AGU Geophys Monogr Ser 168:171–179
Kuvshinov A (2008) 3-D global induction in the oceans and solid Earth: recent progress in modeling magnetic and electric fields from sources of magnetospheric, ionospheric, and oceanic origin. Surv Geophys 29:139–186. doi:10.1007/s10712-008-9045-z
Kuvshinov A, Olsen N (2006) A global model of mantle conductivity derived from 5 years of CHAMP, Ørsted, and SAC-C magnetic data. Geophys Res Lett 33:L18301. doi:10.1029/2006GL027083
Kuvshinov A, Utada H (2010) Anomaly of the geomagnetic Sq variation in Japan: effect from 3-D subterranean structure or the ocean effect? Geophys J Int. doi:10.1111/j.1365-246X.2010.04809.x
Kuvshinov A, Avdeev D, Pankratov O (1999) Global induction by Sq and Dst sources in the presence of oceans: bimodal solutions for non-uniform spherical surface shells above radially symmetric Earth models in comparison to observations. Geophys J Int 137:630–650
Kuvshinov A, Olsen N, Avdeev D, Pankratov O (2002) EM induction in the oceans and the anomalous behavior of coastal *C*-responses for periods up to 20 days. Geophys Res Lett 29(12):1595. doi:10.1029/2001GL014409
Kuvshinov A, Utada H, Avdeev D, Koyama T (2005) 3-D modelling and analysis of Dst *C*-responses in the North Pacific Ocean region, revisited. Geophys J Int 160:505–526
Kuvshinov A, Sabaka T, Olsen N (2006a) 3-D electromagnetic induction studies using the Swarm constellation: Mapping conductivity anomalies in the Earth's mantle. Earth Planets Space 58:417–427
Kuvshinov A, Junge A, Utada H (2006b) 3-D modelling the electric field due to ocean tidal flow and comparison with observations. Geophys Res Lett. doi:10.1029/2005GL025043
Kuvshinov A, Manoj C, Olsen N, Sabaka T (2007) On induction effects of geomagnetic daily variations from equatorial electrojet and solar quiet sources at low and middle latitudes. J Geophys Res 112(B1):0102. doi:10.1029/2007JB004955
Kuvshinov A, Semenov A, Pankratov O, Jackson A, Olsen N (2008) 3-D imaging of mantle conductivity based on inversion of satellite C-responses: Proof of concept. Expanded abstract of 19 Workshop on Electromagnetic Induction in the Earth, Beijing, China
Kuvshinov A, Semenov A, Pankratov O, Olsen N (2009) 3-D mapping of mantle conductivity from space. An approach and its verification. In: Proceedings of 2nd international Swarm science meeting, Potsdam
Kuvshinov A, Velimsky J, Tarits P, Semenov A, Pankratov O, Toffner-Clausen L, Martinec Z, Olsen N, Sabaka T, Jackson A (2010) L2 products and performances for mantle studies with *Swarm*. ESA Final Report, 2010, 173 pp, http://esamultimedia.esa.int/docs/EarthObservation/Induction_Study_150110.pdf

Lizarralde D, Chave A, Hirth G, Schultz A (1995) Long period magnetotelluric study using Hawaii-to-California submarine cable data: implications for mantle conductivity. J Geophys Res 100(B9): 17873–17884

Mackie RL, Madden T (1993) Three-dimensional magnetotelluric inversion using conjugate gradients. Geophys J Int 115:215–229

Manthilake M, Matsuzaki T, Yoshino T, Yamashita S, Ito E, Katsura T (2009) Electrical conductivity of wadsleyite as a function of temperature and water content. Phys Earth Planet Int. doi:10.1016/j.pepi.2008.06.001

Martinec Z (2010) The forward and adjoint methods of global electromagnetic induction for CHAMP magnetic data. In: Freeden W, Nashed MZ, Sonar T (eds) Handbook of geomathematics, pp 565–624. doi:10.1007/978-3-642-01546-5_19

Martinec Z, McCreadie H (2004) Electromagnetic induction modeling based on satellite magnetic vector data. Geophys J Int 157:1045–1060

Martinec Z, Velimsky J (2009) The adjoint sensitivity method of EM induction for CHAMP magnetic data. Geophys J Int 179:1372–1396

Matzka J, Olsen N, Fox Maule C, Pedersen L, Berarducci AM, Macmillan S (2009) Geomagnetic observations on Tristan da Cuhna, South Atlantic Ocean. Ann Geophys 52:97–105

Medin AE, Parker RL, Constable S (2007) Making sound inferences from geomagnetic sounding. Phys Earth Planet Int 160:51–59

Megnin C, Romanowicz B (2000) The three-dimensional shear velocity structure of the mantle from the inversion of body, urface and higher mode waveforms. Geophys J Int 143:709–728

Mochizuki E, YokoyamaY ShimizuI, Hamano Y (1997) Spherical harmonic analysis in terms of unevenly distributed observation points and its applications to geomagnetic data. J Geomag Geoelecr 49:1013–1033

Mosegaard K (1998) Resolution analysis of general inverse problems through inverse Monte Carlo sampling. Inverse Probl 14:405–416

Neal SL, Mackie RL, Larsen JC, Schultz A (2000) Variations in the electrical conductivity of the upper mantle beneath North America and the Pacific Ocean. J Geophys Res 105(B4):8229–8242

Nocedal J, Wright SJ (2006) Numerical optimization. Springer, Berlin

Obayashi M, Sugioka H, Yoshimitsu H, Fukao Y (2006) High temperature anomalies oceanward of subducting slabs at the 410 km discontinuity. Earth Planet Sci Lett 243:149–158

Oganov AR, Ono S (2004) Theoretical and experimental evidence for a postperovskite phase of MgSiO3 in Earth's D'' layer. Nature 430:445–448

Ohta K, Onoda S, Hirose K, Sinmyo R, Shimizu K, Sata N, Ohishi Y, Yasuhara A (2008) The electrical conductivity of post-perovskite in Earth's D" layer. Science 320:89–91

Olsen N (1998) The electrical conductivity of the mantle beneath Europe derived from C-Responses from 3 h to 720 h. Geophys J Int 133:298–308

Olsen N (1999a) Long-period (30 days–1 year) electromagnetic sounding and the electrical conductivity of the lower mantle beneath Europe. Geophys J Int 138:179–187

Olsen N (1999b) Induction studies with satellite data. Surv Geophys 20:309–340

Olsen N, Kuvshinov A (2004) Modelling the ocean effect of geomagnetic storms. Earth Planets Space 56:525–530

Olsen N, Vennerstrøm S, Friis-Christensen E (2002) Monitoring magnetospheric contributions using ground-based and satellite magnetic data. In: Reigber C, Luehr H, Schwintzer P (eds) First CHAMP mission results for gravity, magnetic and atmospheric studies. Springer, New York, pp 245–250

Olsen N, Haagmans R, Sabaka T, Kuvshinov A, Maus S, Purucker M, Rother M, Lesur V, Mandea M (2006) The *Swarm* end-to-end mission simulator study: separation of the various contributions to Earth's magnetic field using synthetic data. Earth Planets Space 58:359–370

Olsen N, Sabaka T, Gaya-Pique (2007) Study of an improved comprehensive magnetic field inversion analysis for *Swarm*. DNSC Scientific Report 1/2007 Danish National Space Center Copenhagen

Olsen N, Mandea M, Sabaka TJ, Toeffner-Clausen L (2009) CHAOS-2—a geomagnetic field model derived from one decade of continuous satellite data. Geophys J Int 23:5–7. doi:10.1111/j.1365-246X.2009.04386.x

Olsen N, Hulot G, Sabaka TJ (2010) Sources of the geomagnetic field and the modern data that enable their investigation. In: Freeden W, Nashed MZ, Sonar T (eds) Handbook of geomathematics, pp 106–124. doi:10.1007/978-3-642-01546-5_5

Pankratov O, Kuvshinov A (2010) General formalism for the efficient calculation of derivatives of EM frequency domain responses and derivatives of the misfit. Geophys J Int 181:229–249

Pankratov O, Avdeev D, Kuvshinov A (1995) Electromagnetic field scattering in a homogeneous Earth: a solution to the forward problem. Phys Solid Earth 31:201–209

Parker RL, Whaler K (1981) Numerical methods for establishing solutions to the inverse problem of electromagnetic induction. J Geophys Res 86:9574–9584
Prieto GA, Parker RL, Thomson DJ, Vernon FL, Graham RL (2007) Reducing the bias of multitaper spectrum estimates. Geophys J Int 171:1269–1281
Riedel K, Sidorenko A (1995) Minimum bias multiple taper spectral estimation. IEEE Trans Signal Process 43:188–195
Roberts RG (1984) The long-period electromagnetic response of the earth. Geophys J R Astr Soc 78:547–572
Rodi W, Mackie RL (2000) Nonlinear conjugate gradients algorithm for 2-D magnetotelluric inversion. Geophysics 66:174–187
Romanowicz B (2003) Global mantle tomography: progress status in the past 10 years. Ann Rev Earth Planet 31:303–328
Sabaka TJ, Olsen N, Purucker ME (2004) Extending comprehensive models of the Earth's magnetic feld with Oersted and CHAMP data. Geophys J Int 159:521–547
Santos FAM, Soares A, Nolasco R, Rodrigues H, Luzio R, Palshin N, ISO-3D Team (2003) Lithosphere conductivity structure using the CAM-1 (Lisbon-Madeira) submarine cable. Geophys J Int 155: 591–600
Schmucker U (1970) Anomalies of geomagnetic variations in the south-western United States. Bull Scripps Inst Ocean, Unif Calif 13:1–165
Schmucker U (1979) Erdmagnetische Variationen und die elektrische Leitfahigkeit in tieferen Schichten der Erde. Sitzungsbericht und Mitteilungen Braunschweigische Wiss Gesellschaft, Sonderheft 4:45–102
Schmucker U (1999a) A spherical harmonic analysis of solar daily variations in the years 1964–1965: response estimates and source fields for global induction - I. Methods. Geophys J Int 136:439–454
Schmucker U (1999b) A spherical harmonic analysis of solar daily variations in the years 1964–1965: response estimates and source fields for global induction—II. Results. Geophys J Int 136:455–476
Schmucker U (2003) Horizontal spatial gradient sounding and geomagnetic depth sounding in the period range of daily variations, In: Protokoll über das Kolloquium Elektromagnetische Tiefenforschung, Königstein, pp 228–237
Schultz A (2010) EMScope: a continental scale magnetotelluric observatory and data discovery resource. Data Sci J 8:IGY6–IGY20
Schultz A, Larsen JC (1987) On the electrical conductivity of the mid-mantle: I. Calculation of equivalent scalar MT response functions. Geophys J R Astr Soc 88:733–761
Schultz A, Pritchard G (1999) A three-dimensional inversion for large scale structure in a spherical domain. In: Spies B, Oristaglio M (eds) Three dimensional electromagnetics. Geophysical Developments Series, vol 7. Society of Exploration Geophysicists, pp 451–476
Schuster A (1889) The diurnal variation of terrestrial magnetism. Phil Trans R Soc Lond A 180:467–518
Semenov V, Jozwiak W (2006) Lateral variations of the mid-mantle conductance beneath Europe. Tectonophys 416:279–288
Semenov A, Kuvshinov A (2010) Spatial distribution of the mantle conductivity as seen from the 3-D inversion of ground-based *C*-responses. Geophysical Research Abstracts 12 EGU2010-12565
Semenov V, Shuman V (2010) Impedances for induction soundings of the Earth' mantle. Acta Geophys 58:527–542
Semenov V, Pek J, Adam A, Jozwiak W, Ladanyvskyy B, Logvinov I, Pushkarev P, Vozar J (2008) Electrical structure of the upper mantle beneath Central Europe: results of the CEMES project. Acta Geophys 56:957–981
Shimizu H, Utada H (1999) Ocean hemisphere geomagnetic network: its instrumental design and perspective for long-term geomagnetic observations in the Pacific. Earth Planets Space 51:917–932
Shimizu H, Koyama T, Baba K, Utada H (2009) Three-dimensional geomagnetic response functions for global and semi-global scale induction problems. Geophys J Int 178:123–144
Shimizu H, Koyama T, Baba K, Utada H (2010a) Revised 1-D mantle electrical conductivity structure beneath the north Pacific. Geophys J Int 180:1030–1048
Shimizu H, Utada H, Baba K, Koyama T, Obayashi M, Fukao Y (2010b) Three-dimensional imaging of electrical conductivity in the mantle transition zone beneath the North Pacific Ocean by a semi-global induction study. Phys Earth Planet Int. doi:10.1016/j.pepi
Singer B (1995) Method for solution of Maxwell's equations in nonuniform media. Geophys J Int 120:590–598
Singer B, Kuvshinov A, Mishina L, Fainberg E (1993) Global geomagnetic sounding: new methodology and results. Phys Solid Earth 29:35–43
Tarits P, Mandea M (2010) The heterogeneous electrical conductivity structure of the lower mantle. Phys Earth Planet Int. doi:10.1016/j.pepi.2010.08.002

Tarits P, Wahr J, Lognonne P (1992) Electrical conductivity heterogeneities in the mantle: correlation with mantle velocity structure. Abstracts of AGU Fall Meeting, San-Francisco
Tarits P, Hautot S, Perrier F (2004) Water in the mantle: results from electrical conductivity beneath French Alps. Geophys Res Lett 31:L06612. doi:10.1029/2003GL019277
Toffelmier DA, Tyburczy JA (2007) Electromagnetic detection of a 410-km-deep melt layer in the southwestern United States. Nature 447:991–994
Toh H, Hamano Y, Ichiki M, Utada H (2004) Geomagnetic observatory operates at the seafloor in the Northwest Pacific Ocean. EOS 85:467, 473
Toh H, Hamano Y, Ichiki M (2006) Long-term seafloor geomagnetic station in the northwest Pacific: A possible candidate for a seafloor geomagnetic observatory. Earth Planets Space 58:697–705
Toh H, Hamano Y, Goto T, Utada H (2010) Long-term seafloor electromagnetic observation in the northwest Pacific may detect the vector geomagnetic secular variation. Data Sci J 9:IGY100–IGY109
Trampert J, Deschamps F, Resovsky J, Yuen D (2004) Chemical heterogeneities throughout the lower mantle. Science 306:853–855
Utada H, Koyama T, Shimizu H, Chave A (2003) A semi-global reference model for electrical conductivity in the mid-mantle beneath the north Pacific region. Geophys Res Lett 30(4):1194–1198. doi:10.1029/2002GL016092
Utada H, Koyama T, Obayashi M, Fukao Y (2009) A joint interpretation of electromagnetic and seismic tomography models suggests the mantle transition zone below Europe is dry. Earth Planet Sci Lett 281:249–257
Uyeshima M, Schultz A (2000) Geoelectromagnetic induction in a heterogeneous sphere: a new 3-D forward solver using a staggered-grid integral formulation. Geophys J Int 140:636–650
Velimsky J (2010) Electrical conductivity in the lower mantle: Constraints from CHAMP satellite data by time-domain EM induction modeling, Phys Earth Planet Int 180(3–4):111–117. doi:10.1016/j.pepi.2010.02.007
Velimsky J, Martinec Z (2005) Time-domain, spherical harmonic-finite element approach to transient three-dimensional geomagnetic induction in a spherical heterogeneous Earth. Geophys J Int 161:81–101
Velımsky J, Martinec Z, Everett ME (2006) Electrical conductivity in the Earth's mantle inferred from CHAMP satellite measurements—I. Data processing and 1-D inversion. Geophys J Int 166:529–542
Vozar J, Semenov V (2010) Compatibility of induction methods for mantle sounding. J Geophys Res 115:B03101. doi:10.1029/2009JB006390
Wang D, Mookherjee M, Xu YS, Karato SI (2006) The effect of hydrogen on the electrical conductivity in olivine. Nature 443:977–980
Weidelt P (1972) The inverse problem of geomagnetic induction. Z Geophys 38:257–289
Weiss CJ (2010) Triangulated finite difference methods for global scale electromagnetic induction simulations of whole mantle electrical heterogeneities. Geochem Geophys Geosyst (submitted)
Xu Y, Poe BT, Shankland TJ, Rubie DC (1998) Electrical conductivity of olivine, wadsleyite, and ringwoodite under upper mantle conditions. Science 280:1415–1418
Yoshino T, Katsura T (2009) Reply to Comments on "Electrical conductivity of wadsleyite as a function of temperature and water content" by Manthilake et al. Discussion. Phys Earth Planet Interiors 174:22–23
Yoshino T, Matsuzaki T, Yamashina S, Katsura T (2006) Hydrous olivine unable to account for conductivity anomaly at the top of the asthenosphere. Nature 443:973–976
Yoshino T, Manthilake G, Matsuzaki T, Katsura T (2008) Dry mantle transition zone inferred from the conductivity of wadsleyite and ringwoodite. Nature 451:326–329